



Petrogenesis of the early Eocene I-type granites in west Yingjiang (SW Yunnan) and its implication for the eastern extension of the Gangdese batholiths

Liyan Ma ^{a,b}, Yuejun Wang ^{a,*}, Weiming Fan ^a, Hongyan Geng ^c, Yongfeng Cai ^{a,b}, Hong Zhong ^d,
Huichuan Liu ^{a,b}, Xiaowan Xing ^{a,b}

^a State Key of Isotope Geochemistry, Guangzhou Institute of Geochemistry, Chinese Academy of Sciences, Guangzhou 510640, China

^b University of Chinese Academy of Sciences, Beijing 100049, China

^c Department of Earth Sciences, the University of Hong Kong, Pokfulam Road, Hong Kong, China

^d State Key Laboratory of Ore Deposit Geochemistry, Institute of Geochemistry, Chinese Academy of Sciences, Guiyang 550002, China



ARTICLE INFO

Article history:

Received 21 December 2012

Received in revised form 9 April 2013

Accepted 29 April 2013

Available online 14 May 2013

Handling Editor: Z.M. Zhang

Keywords:

Zircons U–Pb geochronology

Nd–Hf isotopic composition

I-type gneissic granite

Gangdese belt

West Yingjiang

ABSTRACT

This study reports new zircon U–Pb and Hf isotopes and whole-rock elemental and Sr–Nd isotopic data for the gneissic granite and leucogranite from the Nabang metamorphic zone, Yingjiang area (West Yunnan, SW China). The metamorphosed granitoids crystallized during the early Eocene (~55–50 Ma) with zircons showing $\epsilon_{\text{Hf}}(t)$ values from +11 to –5.3 and crustal model ages of 1.5 to 0.42 Ga, comparable to those of coeval I-type granitoids from the Gangdese batholith, southern Lhasa. The rocks are characterized by metaluminous and weakly peraluminous hornblende-bearing gneissic granites with A/CNK = 0.95–1.09, Na₂O > K₂O, coupled with low initial Sr isotopic values of 0.7049–0.7070 and high $\epsilon_{\text{Nd}}(t)$ values from +1.1 to –7.1. The rocks were derived from crustal materials involving ancient upper crust/sedimentary and juvenile mantle-derived rocks. Together with available data from nearby regions, it is proposed that the early Eocene granitoids in the Nabang and Tengliang area can be correlated to the Gangdese granitoids and represent the southeastward continuation of the magmatic arc resulting from the Neotethyan subduction in southern Tibet. The petrogenesis of early Eocene granitoids in western Yunnan was probably related to the rollback of the subducting Neotethyan slab that caused the remelting of the crustal materials newly modified by the underplated basaltic magma.

© 2013 International Association for Gondwana Research. Published by Elsevier B.V. All rights reserved.

1. Introduction

The continuous northward accretion of a series of exotic blocks and subsequent indentation of India into Asia since the early Cenozoic resulted in the formation of the Tibetan collisional orogen (e.g., Dewey et al., 1988; Yin and Harrison, 2000; Mo et al., 2002; Ding et al., 2005; Pan et al., 2012; Chatterjee et al., 2013). At the southern part of the Lhasa terrane, a giant magmatic belt developed with a length of over 2600 km and width of >100 km during the Cretaceous–Eocene (Fig. 1a). The belt is dominated by the Gangdese batholiths and Linzizong volcanic units that have been regarded as major components of the Andean-type convergent margin associated with the northward subduction of the Neotethyan oceanic lithosphere along the Yarlu-Zangpo suture (e.g., Allegrè et al., 1984; Searle et al., 1987; Harris et al., 1988a; Jiang et al., 1999; Hodges, 2000; Yin and Harrison, 2000; Aitchison et al., 2002; Mo et al., 2005; Chu et al., 2006; Wen et al., 2008a,b; Lee et al., 2009; Zhu et al., 2009a; Zhang et al., 2010c; Zhu et

al., 2011; Guan et al., 2012; Lee et al., 2012; Zhu et al., 2013). However, in the Eastern Himalayan Syntaxis, previous studies have mainly focused on the kinematics and thermogeochronology of the strike-slip faults in the key metamorphic zones involving the Ailaoshan, Chongshan and Gaoligong fault systems (e.g., Tapponnier et al., 1990; Wang and Burchfiel, 1997; Ji et al., 2000a; Socquet and Pubellier, 2005; Searle, 2006; Wang et al., 2006; Song et al., 2010; Zhang et al., 2010a, 2011, 2012). Little attention has been paid to the petrogenesis of igneous rocks in the metamorphic zones in West Yunnan (SW China) prior to the collision of India with Asia and its relationship with the Gangdese batholiths. The geochemical and geochronological data remain sparse so far (e.g., Chen et al., 2006, 2007; Xu et al., 2008; Yang et al., 2009; Xu et al., 2012). As a result, the eastern extension of Gangdese batholith toward one of the metamorphic zones of the Eastern Himalayan Syntaxis is poorly constrained. Furthermore, the timing of the initial collision between India and Asia has also been a hotly debated issue, with three major viewpoints proposed: (1) the Cretaceous to Paleocene (e.g., Jaeger et al., 1989; Burtman, 1994; Liu and Einsele, 1994; Yin and Harrison, 2000; Mo et al., 2002; Zhu et al., 2004; Ding et al., 2005; Yin, 2006; Mo et al., 2007; Mo et al., 2008; Cai et al., 2011; Xia et al., 2011a; Yi et al., 2011; Hu et al., 2012); (2) the Early Eocene (50–55 Ma) (Molnar and Tapponnier, 1975; Patriat and

* Corresponding author at: Guangzhou Institute of Geochemistry, Chinese Academy of Sciences, P.O. Box 1131, Guangzhou 510640, People's Republic of China. Tel./fax: +86 20 85290527.

E-mail address: yjwang@gig.ac.cn (Y. Wang).

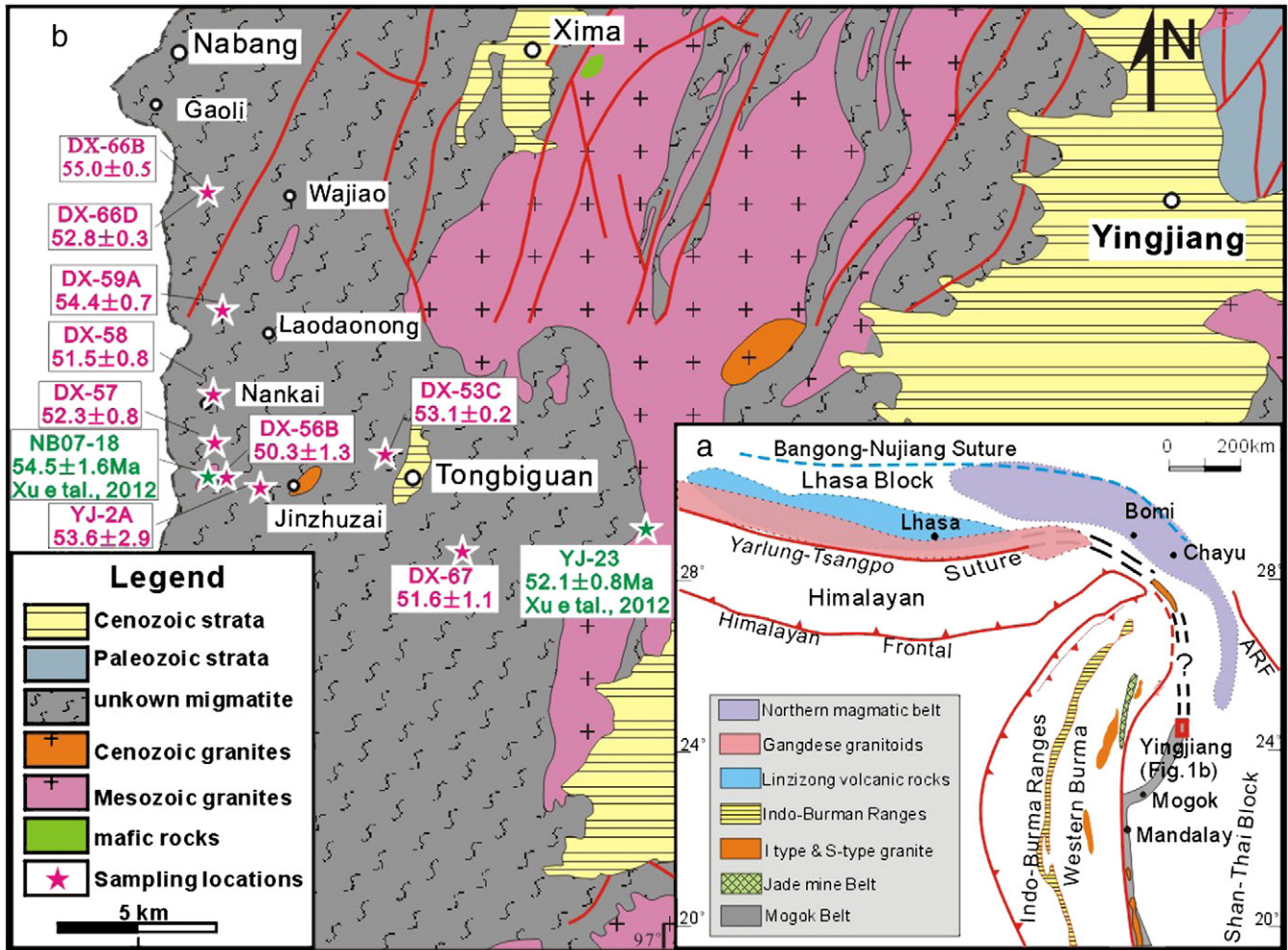


Fig. 1. (a) Schematically tectonic map of the Tibetan Plateau and SE Asia (modified after Mitchell (1993) and Chung et al. (2005)). (b) Geological map of the West Yingjiang area (west Yunnan) (revised from 1:200,000 geological maps of Yingjiang and Ruili). The red and green symbols note the sampling locations for this study and Xu et al. (2012).

Achache, 1984; Searle et al., 1987; Klootwijk et al., 1992; Rowley, 1996; Hodges, 2000; Guillot et al., 2003; Leech et al., 2005; Najman et al., 2005; Garzanti, 2008; Xu et al., 2008; Najman et al., 2010; Wang et al., 2011; Sun et al., 2012); and (3) the Late Eocene (~34–42 Ma) (e.g., Aitchison and Davis, 2001; Aitchison et al., 2007, 2008; Xia et al., 2009; Tan et al., 2010).

To address some of the unresolved issues above, this paper presents a set of new zircon U-Pb geochronological, elemental and Sr-Nd-Hf isotopic data for the gneissic granite and leucogranite from the Nabang metamorphic zone in the Yingjiang area (West Yunnan, SW China). Our focus herein is on the crystallization ages and petrogenesis of these rocks. The results allow us to further discuss the spatial patterns of the Gangdese batholiths and the timing of the initial collision between India and Asia.

2. Geological background and petrology

The west Yingjiang region (West Yunnan) is located geographically to the east of the China–Burma border and tectonically at the Eastern boundary of the Eastern Himalayan Syntaxis (Fig. 1). The region is bounded by the Gaoligong dextral strike-slip fault to the east and the Sagaing fault to the west (e.g., Replumaz and Tapponnier, 2003; Wang et al., 2006). The high-grade metamorphic rocks extensively exposed in this area constitute an important metamorphic zone, named herein as the Nabang metamorphic zone. This zone probably represents the

northern extension of the Mogok metamorphic belt in the eastern Burma Highland, which extends for over 1500 km along the western margin of the Shan–Thai block from the Andaman Sea (Fig. 1a; e.g., Wang, 1983; Mitchell, 1993; Bertrand et al., 1999, 2001; Morley et al., 2001). The early Cretaceous–Eocene mafic–ultramafic rocks in this metamorphic zone are commonly interpreted as ophiolite marking the subduction of the Neotethyan Ocean and subsequent collision of western Burma with Shan–Thai blocks (i.e., Cobbing et al., 1986; Zaw, 1990; Mitchell, 1993; Hughes et al., 2000). Northward, it links to the Gangdese magmatic belt with a length of 2600 km and width of 100 km. The Gangdese belt is composed of the Late Cretaceous–Paleogene Gangdese batholith and Jurassic–Early Cretaceous Northern magmatic (peraluminous S-type granitic) belt (e.g., Xu et al., 1985; Debon et al., 1986; Lee et al., 2003; Chu et al., 2006; Wen et al., 2008b; Guo et al., 2012).

The Nabang metamorphic zone is considered to be a part of the Tengchong block bordered by the dextral Sagaing fault to the west in Burma and Gaoligong shear zone to the east (e.g., Yunnan BGMR, 1990). The block is the northern extension of the Shan–Thai Block of the Cimmerian and was accreted to Eurasia in the late Mesozoic period (Shi et al., 1995; Metcalfe, 1996a,b, 1998; Shi and Archbold, 1998; Ueno, 2003). Its main petrological components include the Gaoligong metamorphic rocks previously mapped as Proterozoic basement, Paleozoic low- to medium-grade metamorphosed sequence, Mesozoic–Tertiary granites and Cenozoic volcanic–sedimentary packages (e.g., Yunnan

BGMR, 1990). The Paleozoic sequences are mainly composed of weakly metamorphosed sandstones, shale/slate and limestone along with the interlayered glacial conglomerate and shale with Gondwana-type cold-water fossil species (e.g., Wang, 1983; Wu et al., 1995; Metcalfe, 1996b; Zhong, 1998; Ueno, 2000).

In the Yingjiang–Nabang areas of the Nabang metamorphic zone, there are abundant high-grade metamorphic rocks. These rocks were traditionally mapped as the “Gaoligong Group” referred to those in the Gaoligong region of the eastern Tengchong Block (Fig. 1a; e.g., Yunnan BGMR, 1990). They are composed of paragneiss, orthogneiss, leucogranite and migmatite with minor amount of mafic-ultramafic granulites in the lower segment and metapelitic, sandstone and slate in the upper segment (e.g., Wang, 1983; Yunnan BGMR, 1990). Recent geochronological studies show that the majority of the orthogneisses and migmatites of the so-called “Gaoligong Group” in the Gaoligong region have variable zircon U–Pb ages with three main age-clusters of ~70–140 Ma, ~200–259 Ma and ~490 Ma, respectively (e.g., Chen et al., 2006; Peng et al., 2006; Wang et al., 2006; Chen et al., 2007; Song et al., 2010; Xu et al., 2012 and references therein). These data suggest that these orthogneisses might not be Precambrian basement as traditionally thought but a suite of gneissic granites. The lentoid mafic-ultramafic rocks along the China–Burma border are geochemically comparable to the MORB basalt, and regarded as the product of the northward subduction of the Neotethyan oceanic lithosphere before the India–Asia collision (e.g., Ji et al., 2000a,c). The associated mafic granulites have an assemblage of garnet + clinopyroxene + plagioclase + amphibole + quartz with the metamorphic pressure of 8–10 kbar and temperature of 750–860 °C (Fig. 1b; Ji et al., 2000a,c).

The gneissic granites extensively occur in the Nabang metamorphic zone and are the fine- to medium-grained biotite granitic, biotite granitic and hornblende-bearing granitic protolith. Part of these rocks was intensely deformed to mylonite, and even ultramylonite, with a sub-vertical foliation and synkinematic minerals (amphibole and

mica) which gave the K–Ar and Ar–Ar ages 10–24 Ma similar to those of the Gaoligong, Jiali and Karakorum shear zones (Searle, 1996; Lee et al., 2003; Wang et al., 2007). The leucogranite truncates the schistosity of the country rocks and commonly shows a medium-to coarse-grained texture with weak foliation.

3. Analytical methods

Zircons were separated by conventional heavy liquid and magnetic techniques and then handpicked under a binocular microscope. After mounting by epoxy, these grains were polished and coated with carbon. The mounts were then photographed in transmitted and reflected light. Their internal texture was examined using cathodoluminescence (CL) imaging using a scanning electron microprobe prior to U–Pb isotopic analyses at the State Key Laboratory of Continental Dynamics (SKLCD), Northwest University (China) and the University of Hong Kong. Measurements of U, Th and Pb isotopes for nine samples were conducted using a Nu Plasma HR MC-ICPMS (Nu Instruments) coupled with an ArF-193 nm laser-ablation system (Resonetics RESOlution M-50-HR) at the University of Hong Kong (DX-66B, DX-66D, DX-53C, DX-67) or an Agilent 7500a quadrupole (Q)-ICPMS attached with a Geolas laser-ablation system equipped with a 193 nm Ar-F-excimer laser at the SKLCD (DX-59A and DX-58, DX-57, DX-56B, and YJ-2A). Analyses were performed with a beam diameter of ca. 30 μm and a repetition rate of 6 Hz, which yielded a signal intensity of 0.03 V for ^{238}U for the standard zircon 91500. Typical ablation time was 40 s for each measurement, resulting in pit depths of 30–40 μm. Masses 232, 208–204 were simultaneously measured in a static-collection mode. External corrections were applied to all unknowns, and standard zircons 91500 and GJ were used as external standards and were analyzed twice before and after every 10 analyses. The instrumental setting and detailed analytical procedure have been described by Yuan et al. (2004) and Xia et al. (2011b). The errors for individual U–Pb analyses are presented with 2σ error in Appendix 1 and in concordia diagrams

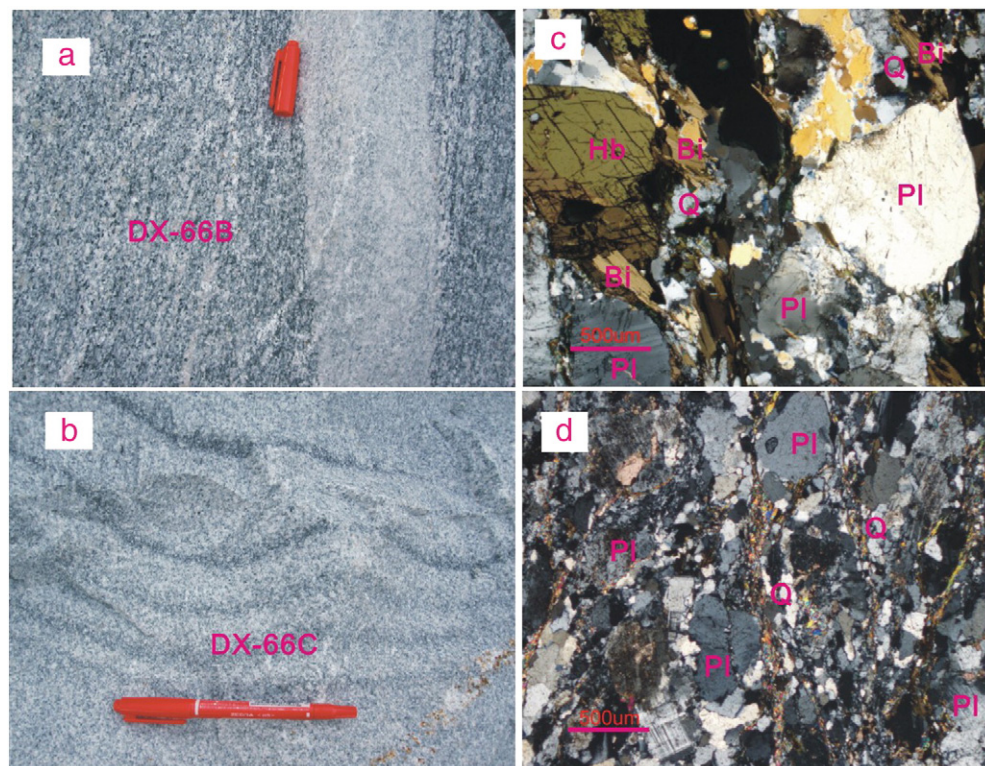


Fig. 2. Outcrop (a–b) and micrographic (c–d) photos of representative gneissic granite samples (DX-66B and DX-67) in west Yingjiang (west Yunnan Province). Pl = plagioclase; Q = quartz; Bi = biotite; Hb = hornblende.

and uncertainties in age results are quoted at a 95 % level (2σ). Raw count rates for ^{29}Si , ^{204}Pb , ^{206}Pb , ^{207}Pb , ^{208}Pb , ^{232}Th and ^{238}U were collected for age determination. Data processing was carried out using ICPMSDataCal 7.2 and Isoplot/Ex 2.49 programs of Ludwig (2001). Zircon in-situ Hf isotopic analysis was carried out using the Nu Instruments MC-ICPMS attached to the Resonetics RESolution M-50-HR Excimer Laser Ablation System at the University of Hong Kong (DX-66B, DX-66D, DX-53C, DX-67), or using a Geolas-193 laser-ablation microprobe attached to a Neptune multi-collector ICP-MS at the SKLCD (DX-57 and DX-58). Analyses were performed with a beam diameter of ca. 55 μm and a repetition rate of 6 Hz, which yielded a signal intensity of 0.04 V at ^{179}Hf for the standard zircon 91500. Typical ablation time was 40 s for each measurement, resulting in pit depths of 30–40 μm . Masses 172–179 were simultaneously measured in static-collection mode. External corrections were applied to all unknowns,

and standard zircons 91500 and GJ were used as external standards and were analyzed twice before and after every 10 analyses. Data were normalized to $^{179}\text{Hf}/^{177}\text{Hf} = 0.7325$, using exponential correction for mass bias. Interference of ^{176}Lu on ^{176}Hf was corrected by measuring the intensity of the interference-free ^{175}Lu isotope and using the recommended $^{176}\text{Lu}/^{175}\text{Lu}$ ratio of 0.02655 (Machado and Simonetti, 2001). The ^{176}Lu decay constant of $1.865 \times 10^{-11} \text{ year}^{-1}$ (Schäfer et al., 2001) was used to calculate initial $^{176}\text{Hf}/^{177}\text{Hf}$ ratios. The chondritic values of $^{176}\text{Hf}/^{177}\text{Hf}$ (0.282772) and $^{176}\text{Lu}/^{177}\text{Hf}$ (0.0332) reported by Blichert-Toft and Albarède (1997) were adopted for the calculation of ϵHf values. The depleted mantle Hf model ages (T_{DM}) were calculated using the measured $^{176}\text{Lu}/^{177}\text{Hf}$ ratios of zircon based on the assumption that the depleted mantle reservoir had a linear isotopic growth from $^{176}\text{Hf}/^{177}\text{Hf} = 0.279718$ at 4.55 Ga to 0.283250 at present, with $^{176}\text{Lu}/^{177}\text{Hf} = 0.0384$ (Griffin et al., 2000). The analytical results for

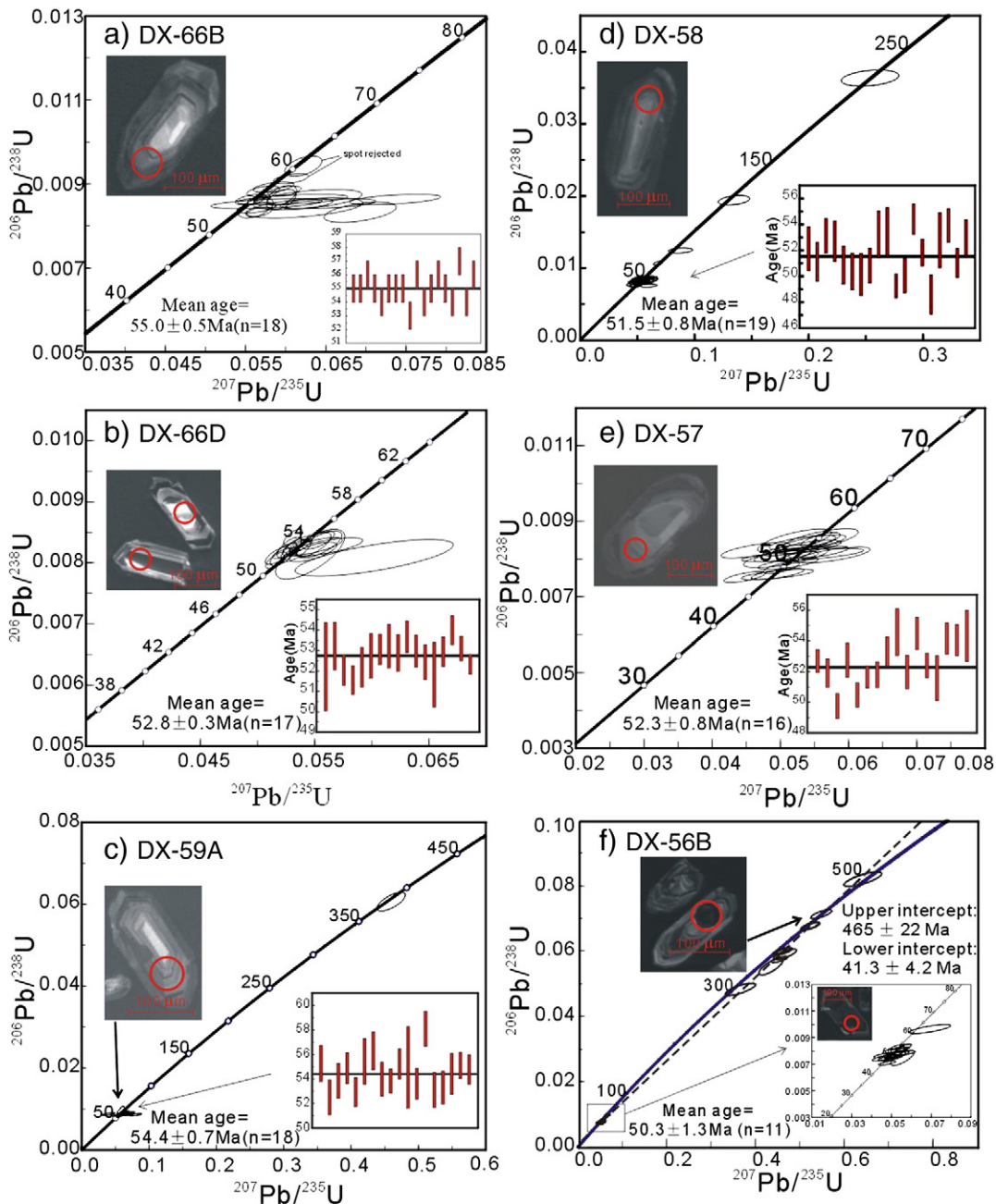


Fig. 3. (a-i) Concordia diagrams of zircon U-Pb data for the gneissic granites and leucogranite from the west Yingjiang area. (a, b) Wajiao (DX-66B and DX-66D), (c) Laodaonong (DX-59A), (d, e) Nankai (DX-57 and DX-58), (f, g) Northern Jinzhuzhai (DX-56B and YJ-2A), (h-i) Tongbiguan (DX-53C and DX-67).

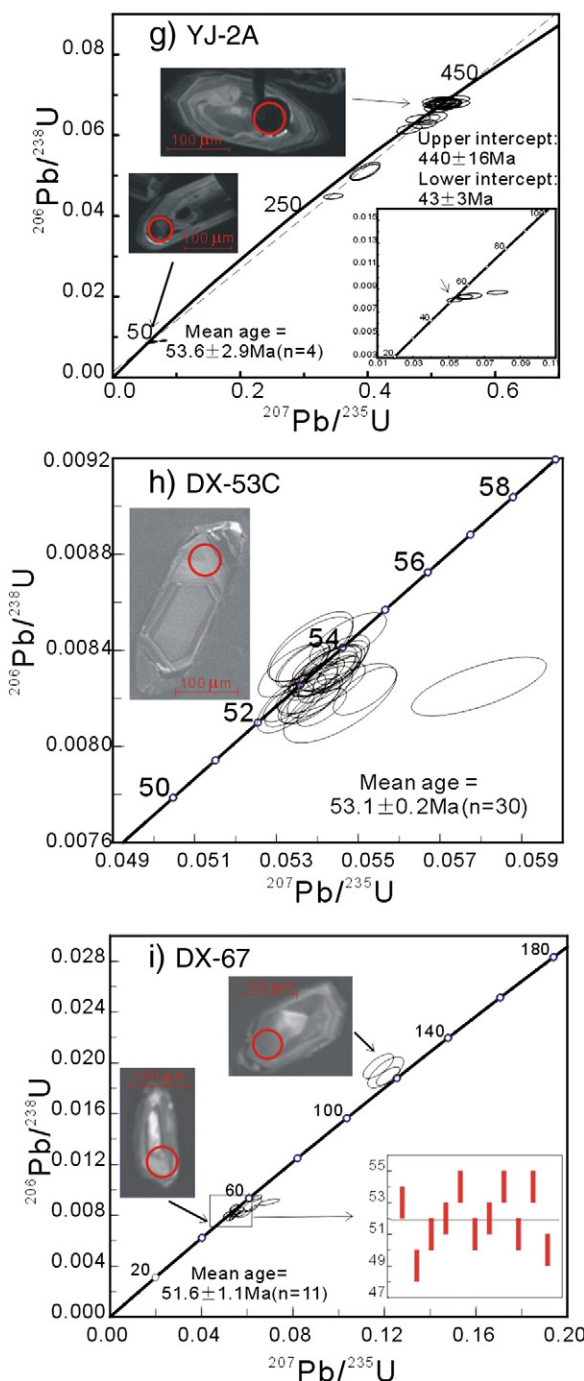


Fig. 3 (continued).

zircon U-Pb and Hf isotopic compositions are listed in Appendix 1, respectively.

The representative samples were crushed to 200-mesh in a steel mortar and ground in a steel mill for the element and isotopic analyses. The whole-rock major oxides were analyzed at the Guangzhou Institute of Geochemistry (GIG), the Chinese Academy of Sciences (CAS) by a wavelength X-ray fluorescence spectrometry using a Rigaku ZSX100e spectrometer. Trace element contents were performed using Perkin-Elmer ScieX ELAN 6000 inductively coupled plasma mass spectrometer (ICP-MS) at the GIG, CAS. The detailed sample preparation and analytical procedures were described by Wei et al. (2002). About 100 mg samples were digested with 1 ml of HF and 0.5 ml HNO₃ in screw top PTFE-lines stainless steel bombs at 190 °C for 12 h. Insoluble residues

were dissolved using 8 ml of 40 % HNO₃ (v/v) heated to 110 °C for 3 h. Samples powders for Sr-Nd isotopic analyses were spiked with mixed isotope tracers, dissolved in Teflon capsules with HF + HNO₃ acids, separated by the conventional cation-exchange technique and run on single W and Ta-Re double filaments. Isotopic ratios were measured on the VG-354 mass-spectrometer at the GIG, CAS. Sample preparation and chemical separation follow Liang et al. (2003). The total procedure blanks for Nd were <50 pg. The mass fractionation corrections for Sr and Nd isotopic ratios are based on $^{86}\text{Sr}/^{88}\text{Sr} = 0.1194$ and $^{146}\text{Nd}/^{144}\text{Nd} = 0.7219$, respectively. The measured $^{87}\text{Sr}/^{86}\text{Sr}$ ratios of the (NIST) SRM987 standard and $^{143}\text{Nd}/^{144}\text{Nd}$ ratios of the La Jolla standard are 0.710265 ± 12 (2σ) and 0.511862 ± 10 (2σ), respectively. Within-run errors of precision for these analyses are estimated to be better than 0.000015 for $^{146}\text{Nd}/^{144}\text{Nd}$ in the 95 % confidence level. The elemental and isotopic results for the representative samples are listed in Appendix 2.

4. Zircon U-Pb dating and Hf isotopic results

Nine gneissic granites and leucogranites along the road from Tongbiguan to Nabang in west Yingjiang (SW Yunnan) were selected for zircon U-Pb dating and Hf isotopic analyses (Fig. 1). These rocks display banding with a strong magmatic preferred orientation or a post-magmatic ductile deformational texture. Their typical mineral assemblage includes plagioclase (~20–40 %), K-feldspar (~10–30 %), quartz (~20–35 %) and biotite (~5–10 %) with minor amounts of hornblende and accessory minerals (e.g., tourmaline, apatite, zircon, monazite and Fe-Ti oxides; Fig. 2a–d). Zircon grains separated from these samples are mostly transparent and euhedral in morphology with a length of about 100 μm. Their internal texture is featured by strong oscillatory zoning with variable luminescence in CL images, typical of a magmatic origin. The sampling location, lithology and analytical results are listed in Appendix 1 and shown in Fig. 3a–i. The results for nine samples are summarized as following.

4.1. DX-66B (gneissic granite) and DX-66D (leucogranite)

Two samples were taken from a creek (N24°42.5', E97°34.754') near Wajiao Village. Zircons from DX-66B have a relatively wide range of Th/U ratios (0.28–0.73) and yield a weighted mean $^{206}\text{Pb}/^{238}\text{U}$ age of 55.0 ± 0.5 Ma with MSWD = 2.2 (n = 18, Fig. 3a). Seventeen spots on 17 grains for DX-66D have the Th/U ratios ranging from 0.28 to 0.68 and form a cluster with the weighted mean $^{206}\text{Pb}/^{238}\text{U}$ age of 52.8 ± 0.3 Ma (MSWD = 2.8, n = 17; Fig. 3b). The corresponding $\epsilon_{\text{Hf}}(t)$ values for DX-66B and DX-66D range from -0.34 to +10 and -4.0 to +11 with Hf crustal model ages of 0.46–1.16 Ga and 0.42–1.38 Ga, respectively (Appendix 1 and Fig. 4a and b).

4.2. DX-59A (hornblende-bearing gneissic granite)

This sample was collected from Laodaonong Village (N24°40.382', E97°35.061). The zircon grains show CL images of typical magmatic zircons and have relatively constant Th/U ratios of 0.46–0.83. They mostly plot on the concordia line and yield the $^{206}\text{Pb}/^{238}\text{U}$ weighted mean age of 54.4 ± 0.7 Ma (MSWD = 3.7, n = 18; Fig. 3c). An exception is the DX-59A-08 spot that has the older $^{206}\text{Pb}/^{238}\text{U}$ apparent age of 379 ± 11 Ma, interpreted as the inherited zircons.

4.3. DX-57 and DX-58 (gneissic granites)

The two samples were collected from the two sites (N24°37.492', E97°34.970' and N24°38.511', E97°34.967') in the Nankai village. The zircons from both samples have Th/U ratios from 0.31 to 1.07. They give the weighted mean ages of 52.51 ± 0.64 Ma (n = 16, MSWD = 6) and 51.5 ± 0.8 Ma (n = 19, MSWD = 6.3), respectively (Fig. 3d and e). These ages are interpreted as the crystallization age of the intrusion.

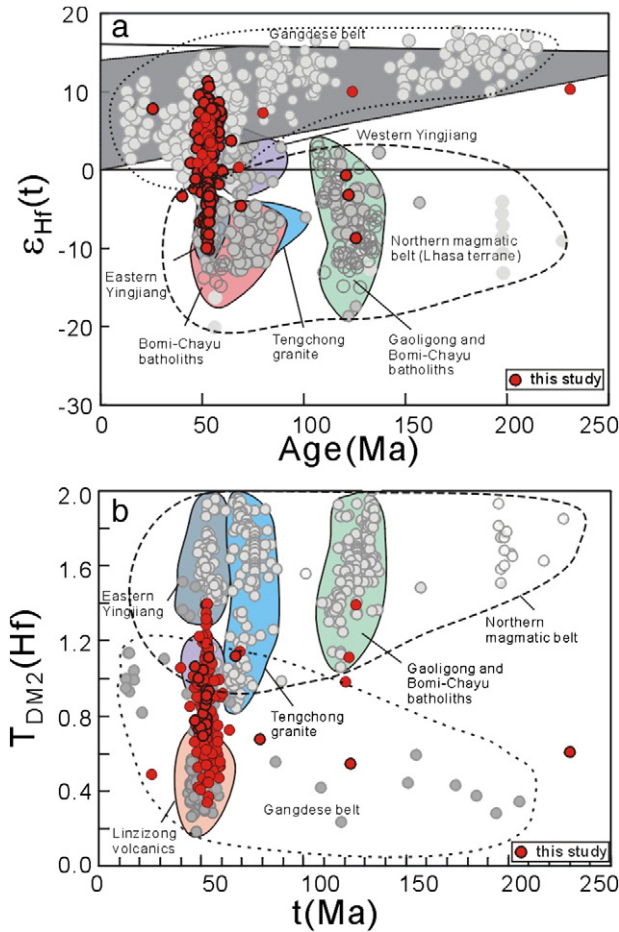


Fig. 4. Age (Ma) vs. $\epsilon_{\text{Hf}}(t)$ (a) and $T_{\text{DM}}(\text{Hf})$ (b) for zircons from gneissic granite samples in west Yingjiang. Also shown are data for the granitoid rocks from the Gangdese belt in Tibet (e.g., Chu et al., 2006; Liang et al., 2008; Chiu et al., 2009; Ji et al., 2009; Mo et al., 2009), the Northern magmatic belt of Lhasa terrane and Tengchong granites (Chiu et al., 2009; Ji et al., 2009; Xu et al., 2012).

Fourteen analyses from DX-57 give $\epsilon_{\text{Hf}}(t)$ values of -4.5 to $+9.4$ and crustal model ages of 0.52 – 1.4 Ga (Appendix 1 and Fig. 4a–b). The corresponding analyses for DX-58 yield positive $\epsilon_{\text{Hf}}(t)$ values ranging from 0.36 to 6.8 with Hf crustal model ages of 0.69 – 1.11 Ga. The core of a zircon grain from DX-58 has the $^{206}\text{Pb}/^{238}\text{U}$ apparent age of 230 ± 6 Ma, representative of the age of inherited zircons.

4.4. DX-56B and YJ-2A (gneissic granites)

The samples are taken from Jinzhuzai village ($N24^{\circ}36.812'$, $E97^{\circ}35.153'$ and $N24^{\circ}36.786'$, $E97^{\circ}35.163'$). Eleven zircon grains with oscillatory zoning from DX-56B show the Th/U ratios of 0.23 to 0.90 and form a cluster with the weighted mean ages of 50.4 ± 1.3 Ma (MSWD = 9.2 , n = 11 , Fig. 3f). A zircon grain (DX-56B-22) gives the oldest apparent $^{206}\text{Pb}/^{238}\text{U}$ age of 509 ± 11 Ma, interpreted as the inherited zircon. The remaining grains plotted below the concordant line but form a well-defined regression line with the upper and lower intercept ages of 465 ± 22 Ma and 41 ± 4 Ma, respectively. Four zircons from YJ-2A have the Th/U ratios of 0.44 to 0.82 and yield the mean $^{206}\text{Pb}/^{238}\text{U}$ age of 53.5 ± 2.9 Ma (Fig. 3g). Another data-cluster is defined by 16 zircons with the $^{206}\text{Pb}/^{238}\text{U}$ apparent ages of 400 Ma to 428 Ma from YJ-2A and give a weighted mean age of 423 ± 1.5 Ma (MSWD = 0.63 , n = 16) with the Th/U ratios of 0.08 – 0.96 . The remaining five zircons yield the relatively younger apparent ages of 282 – 392 Ma and constitute a regression line with the upper and lower intercept ages of 440 ± 16 Ma and 43 ± 3 Ma, respectively.

4.5. DX-53C (leucogranite) and DX-67 (gneissic granite)

Both samples ($N24^{\circ}37.048'$, $E97^{\circ}38.389'$ and $N24^{\circ}35.074'$, $E97^{\circ}41.139'$) are from near Tongbiguan village. All the analyzed grains from the samples show the oscillatory zoning typical of magmatic zircons. Thirty zircons from DX-53C have Th/U ratios ranging from 0.12 to 0.39 and give the $^{206}\text{Pb}/^{238}\text{U}$ apparent ages of 52.4 – 54.0 Ma with the weighted mean age of 53.1 ± 0.2 Ma (MSWD = 3.4) (Fig. 3h). Their in-situ Hf isotopic compositions show the negative $\epsilon_{\text{Hf}}(t)$ values ranging from -10.22 to -1.68 and high Hf crustal model ages ranging from 1.2 to 1.8 Ga (Fig. 4a and b). The fourteen grains from DX-67 cluster at 49.4 – 58.7 Ma with the Th/U ratios of 0.21 – 1.11 and give the weighted mean age of 51.6 ± 1.1 Ma (MSWD = 7.6 , Fig. 3i). The $\epsilon_{\text{Hf}}(t)$ value range from -6.7 to $+0.05$ (average value of -3.9) and the Hf model age from 1.1 Ga to 1.6 Ga (Fig. 4a and b). Three spots including DX-67-03, -04 and -06 yield the $^{206}\text{Pb}/^{238}\text{U}$ apparent ages from 121 Ma to 126 Ma and $\epsilon_{\text{Hf}}(t)$ values from -8.8 to -0.69 (Fig. 4a and b). The remaining DX-67-13 spot gives the oldest $^{206}\text{Pb}/^{238}\text{U}$ apparent age of 447 ± 11 Ma with the negative $\epsilon_{\text{Hf}}(t)$ values of -2.8 , interpreted as inherited grain.

5. Geochemical characteristics

Eight representative samples were selected for elemental and isotopic analyses and the results are presented in Appendix 2. These samples have CIPW compositions of 22.0 – 38.1 % Qz, 10.2 – 45.3 % Or, 15.3 – 38.3 % Ab, 5.0 – 24.9 % An and minor corundum (0 – 1.57 %), and

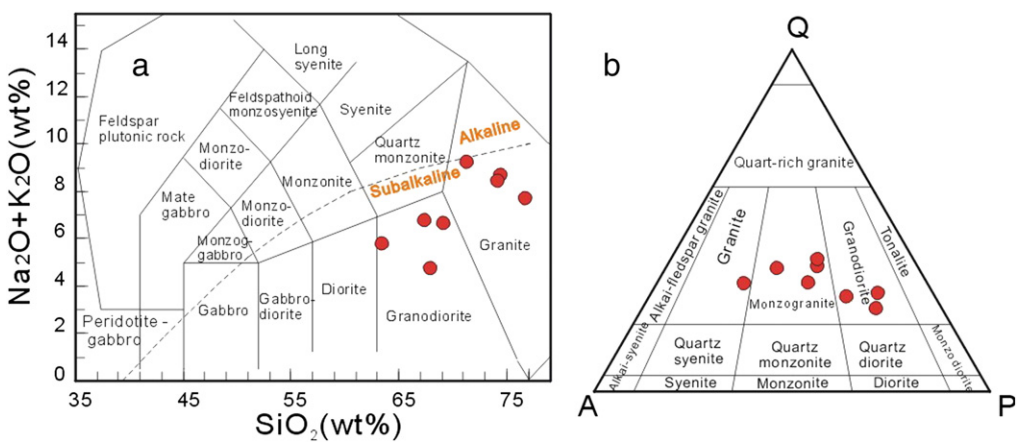


Fig. 5. (a) TAS diagram for classifications of igneous rocks (Middlemost, 1994); (b) QAP diagram for classification of granitoid rocks (Streckeisen, 1976).

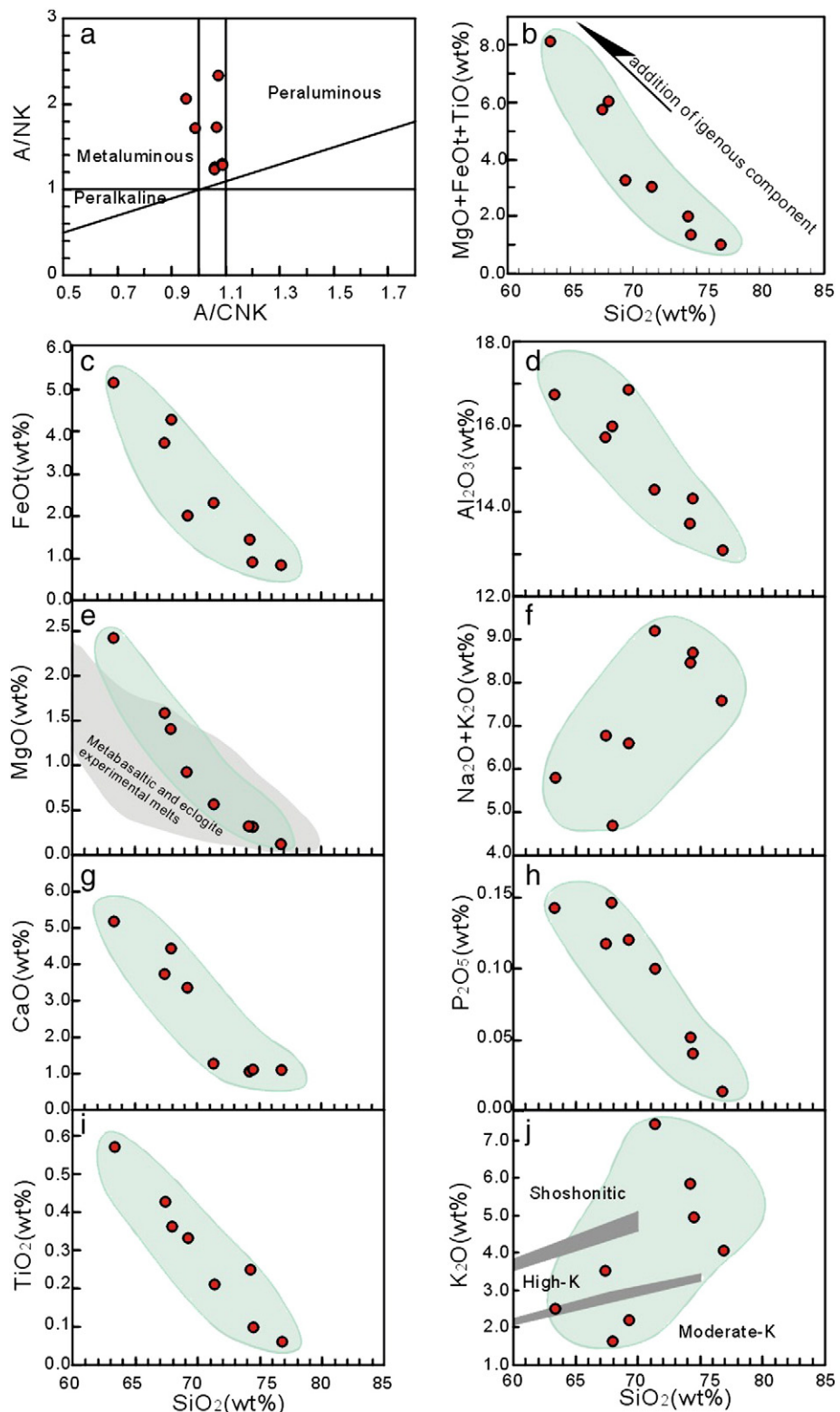


Fig. 6. (a) A/CNK vs. A/NK ; (b–j) SiO_2 vs. $\text{MgO} + \text{FeOt}$, FeOt , Al_2O_3 , MgO , $\text{K}_2\text{O} + \text{Na}_2\text{O}$, CaO , P_2O_5 , TiO_2 and K_2O diagrams for the gneissic granite samples from west Yingjiang. The shaded area in Fig. 6e represents the metabasaltic and eclogite experimental melts (e.g., Rapp and Watson, 1995; Ye et al., 2007). The separating lines in (j) are from Rickwood (1989).

plot in the fields of granite and granodiorite in the TAS diagram and mainly in the field of monzogranite and granodiorite in the QAP diagram (Fig. 5a and b). These samples show 62.71–75.71 wt% of SiO_2 , 12.97–16.79 wt% of Al_2O_3 , 0.14–2.38 wt% of MgO , 0.98–5.63 wt% of FeOt , 1.05–5.11 wt% of CaO , 4.63–9.15 wt% of $\text{K}_2\text{O} + \text{Na}_2\text{O}$. Their A/CNK values (molar $\text{Al}_2\text{O}_3/\text{CaO} + \text{Na}_2\text{O} + \text{K}_2\text{O}$) range from 0.95 to

1.09 (Appendix 2), and can thus be classified as metaluminous to peraluminous granites (Fig. 6a). In the Harker diagram, Al_2O_3 , MgO , CaO , TiO_2 , P_2O_5 , FeOt and $\text{MgO} + \text{TiO}_2 + \text{P}_2\text{O}_5$ correlate negatively with SiO_2 , but a weak positive correlation is observed between SiO_2 and $\text{K}_2\text{O} + \text{Na}_2\text{O}$ (Fig. 6a–i). Such geochemical signatures suggest that plagioclase, biotite and magnetite are the major fractionation phases

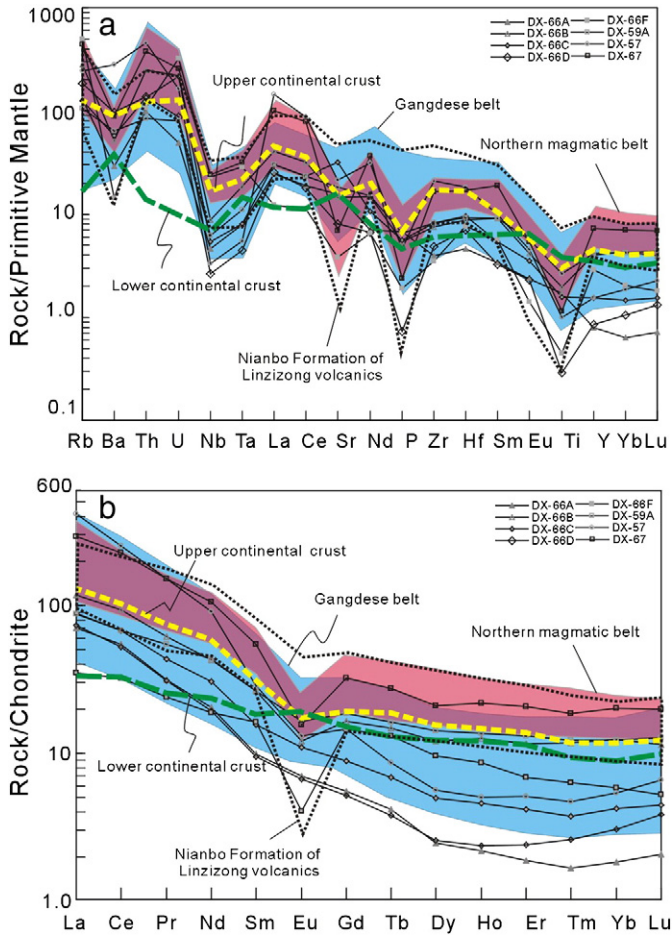


Fig. 7. (a) Primitive mantle-normalized elemental patterns and (b) chondrite-normalized REE patterns for the gneissic granite samples in west Yingjiang. Normalized values for chondrite and primitive mantle are from Taylor and McLennan (1985) and Sun and McDonough (1989), respectively. Also shown are the patterns for the granitoid rocks from the Gangdese belt (Debon et al., 1986; Harris et al., 1988a; Huang et al., 2010), the Nianbo Formation of the Linzizong volcanic rocks (e.g., Li et al., 2008; Mo et al., 2008; Xie et al., 2011; Lee et al., 2012), and granitoid rocks from the Northern magmatic belt (e.g., Harris et al., 1988a; Zhu et al., 2009b; Zhang et al., 2010b; Huang et al., 2012). The upper continental crust and lower continental crust are from Rudnick and Gao (2003).

in the magma evolution (e.g., Wilson, 1989). In the SiO_2 versus K_2O diagram, these samples plot in a wide field with moderate-K, high-K and shoshonitic series (e.g., Rickwood, 1989).

On the primitive mantle-normalized spidergram (Fig. 7a), the samples exhibit a “spiky” pattern with strong negative Ba, Nb-Ta, P and Ti anomalies and variable Sr anomalies, generally similar to those of the global average upper crust (e.g., Rudnick and Gao, 2003). Such a pattern is also consistent with that of the Gangdese granite (e.g., Debon et al., 1986; Harris et al., 1988a; Huang et al., 2010). The studied samples exhibit total REE contents of 51–322 ppm, with $(\text{La/Yb})_{\text{cn}} = 5.99\text{--}77.5$, $(\text{Gd/Yb})_{\text{cn}} = 1.32\text{--}3.02$, and $\text{Eu/Eu}^* = 0.26\text{--}0.95$ (Appendix 2). They show a steeply right-sloping chondrite-normalized pattern, resembling to that of the Gangdese granite (Fig. 7b; Debon et al., 1986; Harris et al., 1988a; Huang et al., 2010). Several samples show a concave-upward REE pattern with more depleted MREE relative to LREE and HREE (e.g., DX-66C), suggestive of hornblende fractionation (e.g., Frey et al., 1978; Klein et al., 1997; Bottazzi et al., 1999).

The studied samples have initial $^{87}\text{Sr}/^{86}\text{Sr}$ ratios between 0.7050 and 0.7070 and $\varepsilon_{\text{Nd}}(t)$ values from -7.1 to $+1.1$, with the Nd model ages of 0.63–2.2 Ga (Appendix 2). Such isotopic compositions are consistent with those of the Gangdese granites (Debon et al., 1986; Harris et al., 1988b; Wen et al., 2008a; Huang et al., 2010) and the Lachlan I-type granites (Healy et al., 2004), but distinct from those of the Northern

magma belt, Tengchong and Baoshan terranes and the Lachlan S-type granites in eastern Australia (e.g., Healy et al., 2004; Wang et al., 2007; Liu et al., 2009; Yang et al., 2009).

6. Discussion

6.1. Magma source with voluminous input of a juvenile component

The geochemical characteristics of the gneissic granite samples in the Nabang metamorphic zone described above indicate that these rocks are typical peraluminous I-type granitoids (Chappell and White, 1974, 2001). Several samples contain amphibole and can be classified as amphibole-rich calc-alkaline granites. These rocks can be produced by the fractional crystallization of a mantle-derived low-K basaltic magma (e.g., Singer et al., 1992; Barth et al., 1995). Our samples show a decrease of FeO^t , MgO , Al_2O_3 , CaO , Sr , Eu/Eu^* and Dy/Yb with an increase in SiO_2 , suggesting significant fractional crystallization of plagioclase, K-feldspar, hornblende and biotite during magma evolution (Figs. 6c–e, g and 8a–c). Further evidence suggesting the removal of plagioclase, K-feldspar and biotite includes: 1) Ba increases with the increasing Sr (Fig. 8b); 2) Rb content decreases with the decrease of Sr (Fig. 8a); and 3) depletion of Ba and Eu (Fig. 7a and b). Apatite and Fe-Ti oxides might have been removed from the magma, as indicated by the negative correlations between SiO_2 and P_2O_5 and TiO_2 , as well as the negative P and Ti anomalies (Fig. 7a). However, the majority of the analyzed samples are characterized by metaluminous and weakly peraluminous signature and high $\text{K}_2\text{O}/\text{Na}_2\text{O}$ ratios (0.5–4.2). The $\text{CaO}/\text{Al}_2\text{O}_3$ ratio decreases with magma evolution. These observations contradict to what would be expected for the fractionation of the mantle-derived low-K basaltic magma in a closed system (e.g., Zen, 1986; Gaudemer et al., 1988). In addition, the samples show wide variations in whole-rock Sr-Nd and zircon in-situ Hf isotopic compositions (Appendices 1 and 2), against the petrogenetic model by simple fractionation of the mantle-derived low-K basaltic magma.

The majority of the samples shows $\varepsilon_{\text{Nd}}(t)$ values ranging from -2.0 to $+1.1$ and Nd model ages of 0.63–0.94 Ga. The zircon initial Hf isotopic ratios of 102 grains with the Eocene crystallization ages yield the $\varepsilon_{\text{Hf}}(t)$ values of -10 to $+11$, which display a bimodal distribution with the peak values being at -3 and $+6$ (Fig. 9a). The Hf model ages range from 0.42 Ga to 1.4 Ga, with the clusters of 0.75 Ga and 1.32 Ga (Fig. 9b). Such Hf-Nd isotopic compositions are distinct from those of the Gaoligong and Tengliang batholiths that were interpreted as the derivation of the metasedimentary rocks (e.g., Xu et al., 2012). In contrast, these signatures are in agreement with those of the Gangdese batholiths that are commonly regarded as remelting products of the lower crust with a significant involvement of a juvenile component (Fig. 10a and b; e.g., Chappell and White, 1974; Pitcher, 1982; Jiang et al., 1999; Mo et al., 2005; Chu et al., 2006; Wen et al., 2008b; Lee et al., 2012 and references therein). The similarity of their MgO contents with the experimental liquids of basaltic amphibolite at a comparable content of SiO_2 suggests that their petrogenesis is related to a basaltic source (e.g., Rapp and Watson, 1995). These samples have relatively high $\text{CaO}/\text{Na}_2\text{O}$ and $\text{CaO}/(\text{MgO} + \text{FeO}^t)$ but low $\text{Al}_2\text{O}_3/\text{TiO}_2$, $\text{Al}_2\text{O}_3/(\text{MgO} + \text{FeO}^t)$, Rb/Ba and Rb/Sr ratios, consistent with what would be expected for the basalt-derived rocks (Fig. 11a–d; e.g., Sylvester, 1998; Altherr et al., 2000; Anthony, 2005). This indicates the important contribution of the basaltic component in the magma source. Our data show that over 50% zircons from the Nabang gneissic granites have positive $\varepsilon_{\text{Hf}}(t)$ values of greater than $+4$, with the highest $\varepsilon_{\text{Hf}}(t)$ value being up to $+11$, indicating a significant involvement of a juvenile basaltic component for the magma source (e.g., Harris et al., 1988b; Jiang et al., 1999; Mo et al., 2005; Chu et al., 2006; Wen et al., 2008b; Chiu et al., 2009). Such a contribution is also evidenced by the coeval gabbroic intrusions in the study area (authors' unpublished data). In the plot of $\varepsilon_{\text{Nd}}(t)$ and $\varepsilon_{\text{Hf}}(t)$ values (Fig. 10b), the early Eocene grains fall into the field of the Gangdese batholith. Their Sr-Nd isotopic

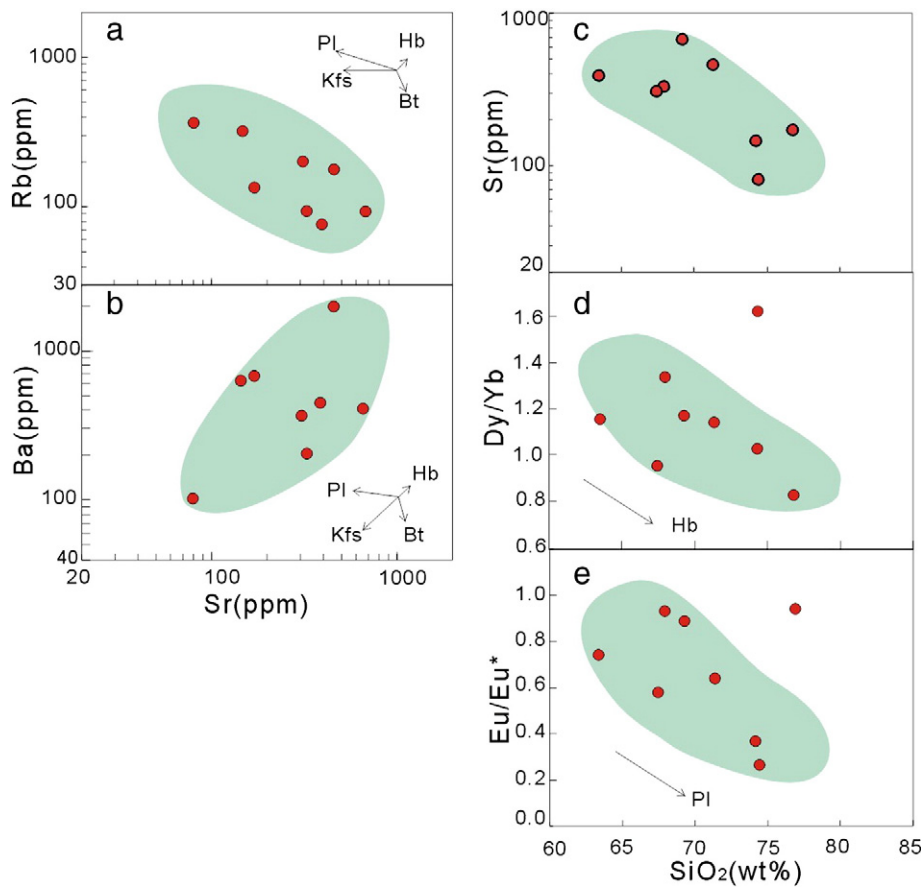


Fig. 8. The plots of Sr vs. Rb (a) and Ba (b) for gneissic granite samples from west Yingjiang showing the trending of fractional crystallization. (c–e) SiO_2 vs. Sr (c), Dy/Yb (d) and Eu^* (e) diagrams showing the fractional crystallization of hornblende and plagioclase.

ratios are identical with those of the Gangdese batholith (e.g., Debon et al., 1986; Harris et al., 1988b; Wen et al., 2008a; Huang et al., 2010), and plot along the depleted mantle-derived magma and Northern magmatic belt (Fig. 10a). In addition, the highly positive $\varepsilon_{\text{Hf}}(t)$ values of the Eocene Nabang gneissic granites decrease sharply to negative values towards east into the Tengliang areas (Fig. 12). Such a spatial variation in the Hf isotopic composition is consistent with the lithological variation of I-type granites in the Nabang and metasediment-derived S-type granites in the Northern magmatic belt of the Lhasa and Tengliang granitoids of the Tengchong Blocks (e.g., Harris et al., 1990; Chung et al., 2005; Kapp et al., 2005; Xu et al., 2012). The presence of the inherited grains also suggests the involvement of ancient crustal materials for the petrogenesis of the Nabang gneissic granites. In summary, our data suggest that the magma source of the Nabang gneissic granites most likely involved ancient sedimentary and juvenile basaltic rocks.

6.2. Temporal and spatial comparison with the Gangdese batholith

Numerous data support the development of two magmatic belts in the Lhasa Block involving the Gangdese belt and Northern magmatic belt (e.g., Chung et al., 2005; Chu et al., 2006; Wen et al., 2008b). The Gangdese belt is predominantly characterized by the I-type batholiths that formed at ~103–80 and 69–34 Ma (age-peak at ~50 Ma; e.g., Wen et al., 2008b; Ji et al., 2012 and references therein). The batholiths might have been derived through the underplating of juvenile basaltic rocks in an Andean-type magmatic belt along the Asian continental margin, as evidenced by the positive whole-rock $\varepsilon_{\text{Nd}}(t)$ and zircon $\varepsilon_{\text{Hf}}(t)$ values. The Northern magmatic belt is dominated by peraluminous S-type granites with negative $\varepsilon_{\text{Nd}}(t)$ and $\varepsilon_{\text{Hf}}(t)$ values that are genetically linked to metasedimentary sequences

(Harris et al., 1990; Chung et al., 2005; Kapp et al., 2005; Chiu et al., 2009; Xu et al., 2012). A possible scenario is that the magmatic activity temporally spanned over the Triassic to early Cretaceous with intensification at 110–130 Ma, in contrast with that of the Gangdese batholith. However, whether the two magmatic belts, especially the Gangdese batholith, extend southward beyond the eastern Himalayan Syntaxis on the China–Burma border remains unknown. Our data provide the possibility for the temporal and spatial comparison for the Gangdese batholith and Nabang metamorphic zone.

The gneissic granites in this study are the important components of the Nabang metamorphic zone and have been previously mapped as the Proterozoic “Gaoligong” sequences (e.g., Yunnan BGMR, 1990). The zircons from these samples give the weighted mean $^{206}\text{Pb}/^{238}\text{U}$ ages of 55.0 Ma (DX-66B), 52.8 Ma (DX-66D), 54.4 Ma (DX-59A), 51.5 Ma (DX-58), 52.3 Ma (DX-57), 53.6 Ma (YJ-2A), 50.3 Ma (DX-56B), 53.1 Ma (DX-53C) and 51.6 Ma (DX-67) (Figs. 1 and 3), interpreted as the crystallization ages of the samples. These data indicate that the so-called Precambrian granitic gneiss and leucogranite are of earliest Eocene (50–55 Ma) age. Geochemically, they can be regarded as the I-type granites with a voluminous input of the juvenile mantle-derived component in the magma source. The relatively low $\varepsilon_{\text{Hf}}(t)$ values for the Nabang I-type gneissic granites compared with those for the typical Gangdese batholith may suggest the involvement of higher proportional sedimentary component for the Nabang granitic magma. From the Tengchong–Lianghe and Gaoligong areas to the east of the Nabang metamorphic zone, late Cretaceous–Paleogene (~120–50 Ma) S-type granites occur extensively with markedly negative $\varepsilon_{\text{Nd}}(t)$ and $\varepsilon_{\text{Hf}}(t)$ values, which Xu et al. (2012) correlated to the involvement of ancient metasedimentary rocks. The synthesis of these data suggests the development of the I- and S-type magmatic

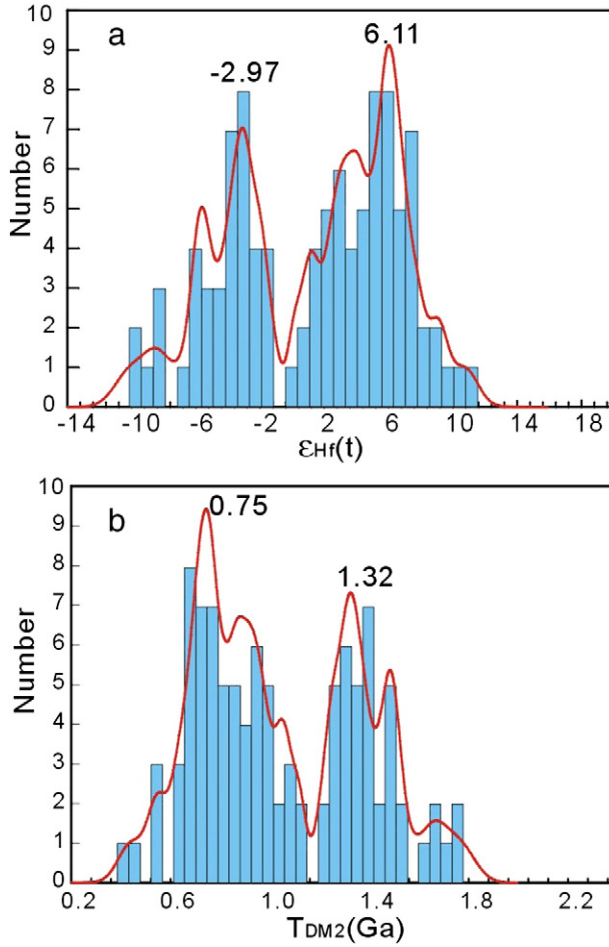


Fig. 9. Frequency of (a) $\epsilon_{\text{Hf}}(t)$ values and (b) Hf model ages for gneissic granite samples from the Nabang area in west Yunnan.

zones with contrasting Nd-Hf isotopic compositions in the western (Nabang-Yingjiang) and eastern (Tengliang-Gaoligong) areas of the Tengchong Block. Such a temporal-spatial pattern for the lithologic affinity and Nd-Hf isotopic compositions in the Nabang and Tengliang areas are comparable to those of the Gangdese batholith and Northern magmatic belt of the Lhasa Block in Tibet, and also resemble those for the coastal margin arc belt and inland peraluminous granite belt in the North American Cordillera (e.g., Mitchell, 1981; Ducea, 2001). This indicates a similar tectonic evolution for the Tengchong and Lhasa blocks and comparable magmatism for the Nabang-Tengliang and Gangdese areas before the India-Asia collision (e.g., Metcalfe, 1998). It can be further concluded that the magmatism in the Nabang-Tengliang areas represents the eastward continuation of the magmatism of the Lhasa block and that the Nabang (Yingjiang) earliest Eocene I-type gneissic granites are most likely the equivalent of the Gangdese arc magmatic rocks (e.g., Xu et al., 2012). The Tengchong Block is tectonically an extruded block (e.g., Mitchell, 1993; Wang et al., 2006; Searle et al., 2007). Its extruded western boundary might be represented by the dextral strike-slip shearing system in the Mogok metamorphic belt beyond the eastern Himalayan Syntaxis (e.g., Ji et al., 2000b; Wang et al., 2006). Therefore, the earliest Eocene Nabang I-type granitic zone might extend further south to Sumatra along the Mogok metamorphic belt in eastern Burma (e.g., Mitchell, 1993; Barley et al., 2003).

6.3. A petrogenetic model for Neotethyan subduction

As mentioned above, the 50–55 Ma Nabang gneissic granites show an I-type geochemical affinity, low $^{87}\text{Sr}/^{86}\text{Sr}$ ratios and high $\epsilon_{\text{Nd}}(t)$ and

$\epsilon_{\text{Hf}}(t)$ values, representing a remelting product of crustal materials with a significant addition of the juvenile basaltic component. This suggests a two-stage process for the petrogenesis of the gneissic granites, involving underplating of mantle-derived magma into the ancient metasedimentary units and subsequent anatexis of the mixed source. Available data show that the continuous northward accretion of the Burma Block probably occurred during the Jurassic to Paleocene time (e.g., Mitchell, 1993; Chung et al., 2005; Chu et al., 2006; Xu et al., 2012). The reported data show the presence of latest Cretaceous (~74 Ma) mafic-ultramafic rocks with MORB-like geochemical affinity ($\epsilon_{\text{Nd}}(t)$ values from +4.9 to +9.6) at Nabang (Ji et al., 2000c and authors' unpublished data), suggesting that the basaltic underplating probably occurred during the latest Cretaceous-Paleocene period (~60–70 Ma). The palaeomagnetic observations show that the northward drift of the Indian plate sharply decelerated to 4.5 cm/y from 18–19 cm/y at earliest Eocene (Klootwijk et al., 1992). The stratigraphic signatures and related metamorphism indicate that the Indian continental crust reached the Transhimalaya at ~50 Ma (Garzanti et al.,

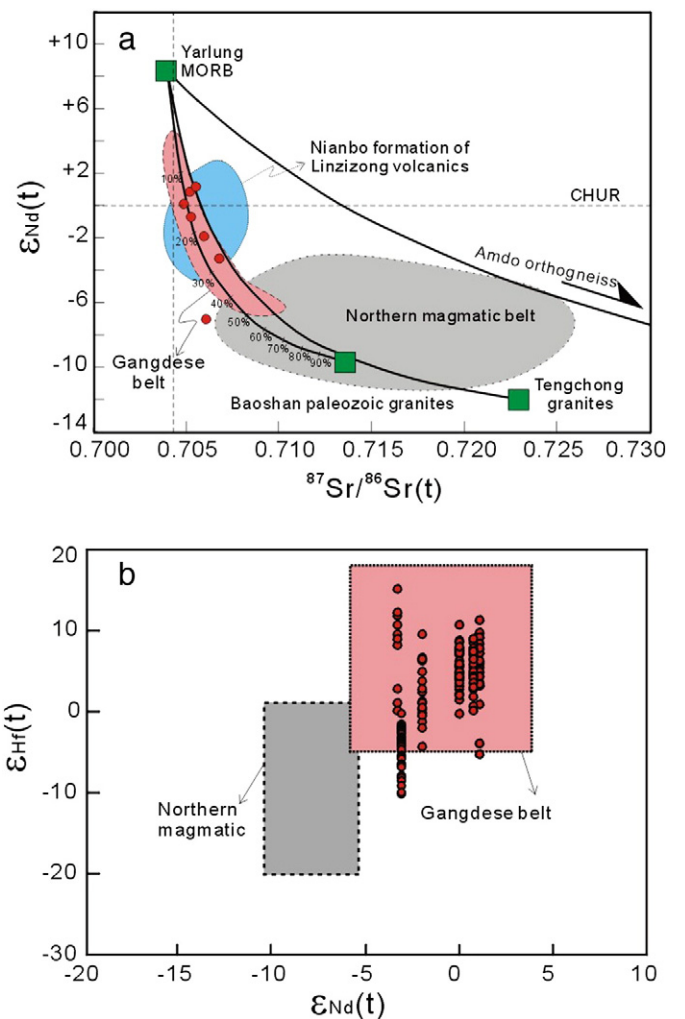


Fig. 10. (a) Initial Sr-Nd isotopic composition and (b) $\epsilon_{\text{Nd}}(t)$ vs. $\epsilon_{\text{Hf}}(t)$ for gneissic granite samples from west Yingjiang. Also shown in (a) are the data for granitoid rocks from the Gangdese belt (i.e., Debon et al., 1986; Harris et al., 1988b; Wen et al., 2008a; Huang et al., 2010) and from the Northern magmatic belt (i.e., Zhu et al., 2009b; Zhang et al., 2010b; Huang et al., 2012), and the Nianbo Formation of the Linzizong volcanic rocks in Tibet (i.e., Mo et al., 2008; Xie et al., 2011; Lee et al., 2012). In (b), the pink and gray fields note those from the Gangdese belt and the Northern magmatic belt (Harris et al., 1988b; Chiu et al., 2009; Mo et al., 2009; Zhu et al., 2009b; Huang et al., 2010; Zhang et al., 2010b; Huang et al., 2012).

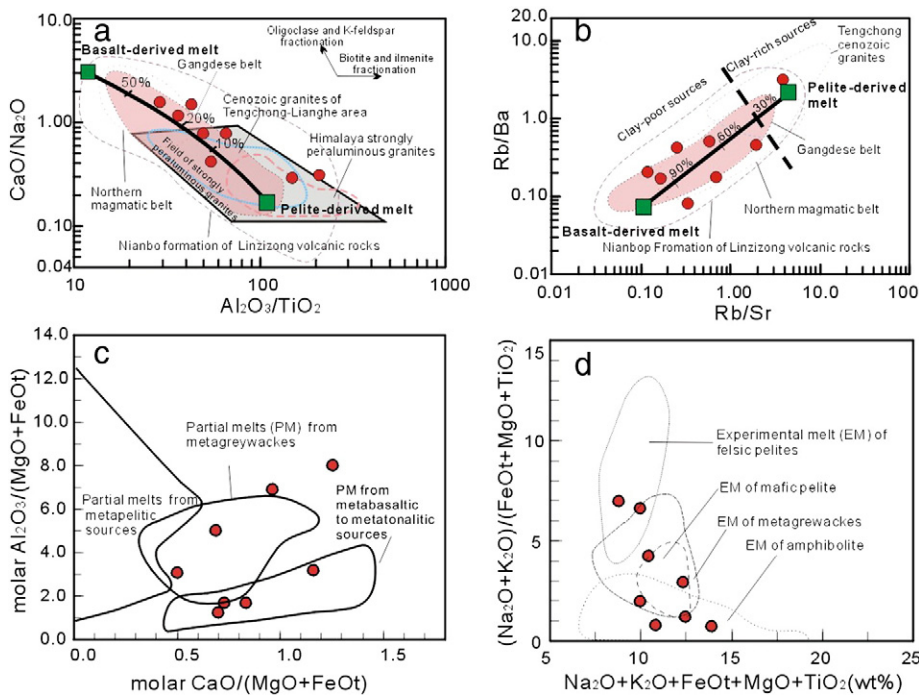


Fig. 11. (a) $\text{Al}_2\text{O}_3/\text{TiO}_2$ vs. $\text{CaO}/\text{Na}_2\text{O}$, (b) Rb/Sr vs. Rb/Ba , (c) molar $\text{Al}_2\text{O}_3/(\text{MgO} + \text{FeOt})$ vs. Molar $\text{CaO}/(\text{MgO} + \text{FeOt})$, and (d) $(\text{Na}_2\text{O} + \text{K}_2\text{O})/(\text{FeOt} + \text{MgO} + \text{TiO}_2)$ vs. $\text{Na}_2\text{O} + \text{K}_2\text{O} + \text{FeOt} + \text{MgO} + \text{TiO}_2$. The data for granitoid rocks in Gangdese are from Debon et al. (1986), Harris et al. (1988a) and Huang et al. (2010) and those for the Nianbo Formation of the Linzizong volcanic rocks are from Li et al. (2008), Xie et al. (2011), Mo et al. (2008) and Lee et al. (2012). The data for granitoids in the Northern magmatic belt are from Zhang et al. (2010b), Zhu et al. (2009b) and Huang et al. (2012) and those of the Cenozoic granites of the Tengchong area are from Yang et al. (2009). Other fields in (a-d) are from Douce and Harris (1998a), Sylvester (1998), Douce (1999) and Altherr et al. (2000).

1987; Searle et al., 1987; Leech et al., 2005; Najman et al., 2010; Wang et al., 2011). In combination with other data from Klootwijk et al. (1992), Hedges (2000), Najman et al. (2005, 2010) and Xu et al. (2008), it is most likely that the India–Asia collision commenced at ~50–55 Ma or later. Thus the dominant input of the juvenile mantle-derived magma should be genetically associated with a subduction rather than intra-crustal thickening setting.

On the discrimination diagrams of Rb–Hf–Ta, Rb–Yb + Ta, Rb–Y + Nb, Ta–Yb and Nb–Y (e.g., Harris et al., 1986; Pearce et al., 1984), our samples plot in the field of arc volcanics (Fig. 13a–f). Taking into account the geochemical similarity with the Gangdese batholiths, we propose that the earliest Eocene (50–55 Ma) Nabang

I-type gneissic granites formed in the transition setting from the northward subduction of the Neotethyan slab to initial collision between India and Asia, as also proposed for the Gangdese batholith and Linzizong volcanic sequences in the Lhasa Block (e.g., Lee et al., 2009, 2012). The syntheses of these data indicate that the initiation of the India–Asia collision should not be earlier than ~55 Ma. This is further supported by the metamorphic age of 40–47 Ma for the lenticular high-temperature, high-pressure granulites ($T = 750$ – 860°C , $P = 0.8$ – 1.0 GPa, Ji et al., 1998, 2000a) and amphibolites ($T = 650$ – 720°C , $P = 0.59$ – 0.80 GPa, Ji et al., 1998, 2000a) with an affinity to Gangdese arc magmatism along the eastern Himalayan Syntaxis (e.g., Nabang, Mogok, Namche Barwa; Ding and Zhong, 1999; Hughes et al., 2000; Ding et al., 2001; Kohn and Parkinson, 2002; Barley et al., 2003; Gao et al., 2008; Xia et al., 2009; Zhang et al., 2010d and authors' unpublished data). In the Tengliang and Gaoligong area, the Eocene (40–42 Ma) mafic dykes show an intraplate geochemical affinity, and were derived from the asthenosphere/enriched lithosphere mantle in response to break off of the subducted slab (Xu et al., 2008). Together with available data, a petrogenetic model is herein proposed for the earliest Eocene Nabang gneissic granites. At >60 Ma, the Neotethyan slab is subducted northwardly beneath the Asian continent to generate a magmatic arc behind the fore-arc basin along the Nabang area on the China–Burma border. Such a process resulted in the basaltic magma underplating at the base of the crust and formed a mixed source with ancient metasedimentary sequences. At ~50–55 Ma, the subducted Neotethyan slab became steepened to stimulate the rollback of the slab. Such a mechanism facilitated the downward drag of the slab to greater depths and the remelting of the crustal materials newly modified by the underplated basaltic magma. As a result, the formation of the earliest Eocene Nabang I-type gneissic granites was closely related to the Neotethyan subduction beneath the Eastern Burma Highlands and Tengchong Block.

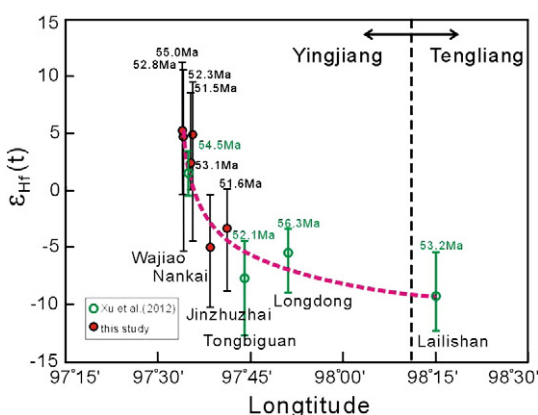


Fig. 12. The spatial variation of average $\epsilon_{\text{Hf}}(t)$ for zircons from the early Eocene granitic samples from west Yingjiang across Tengliang area.

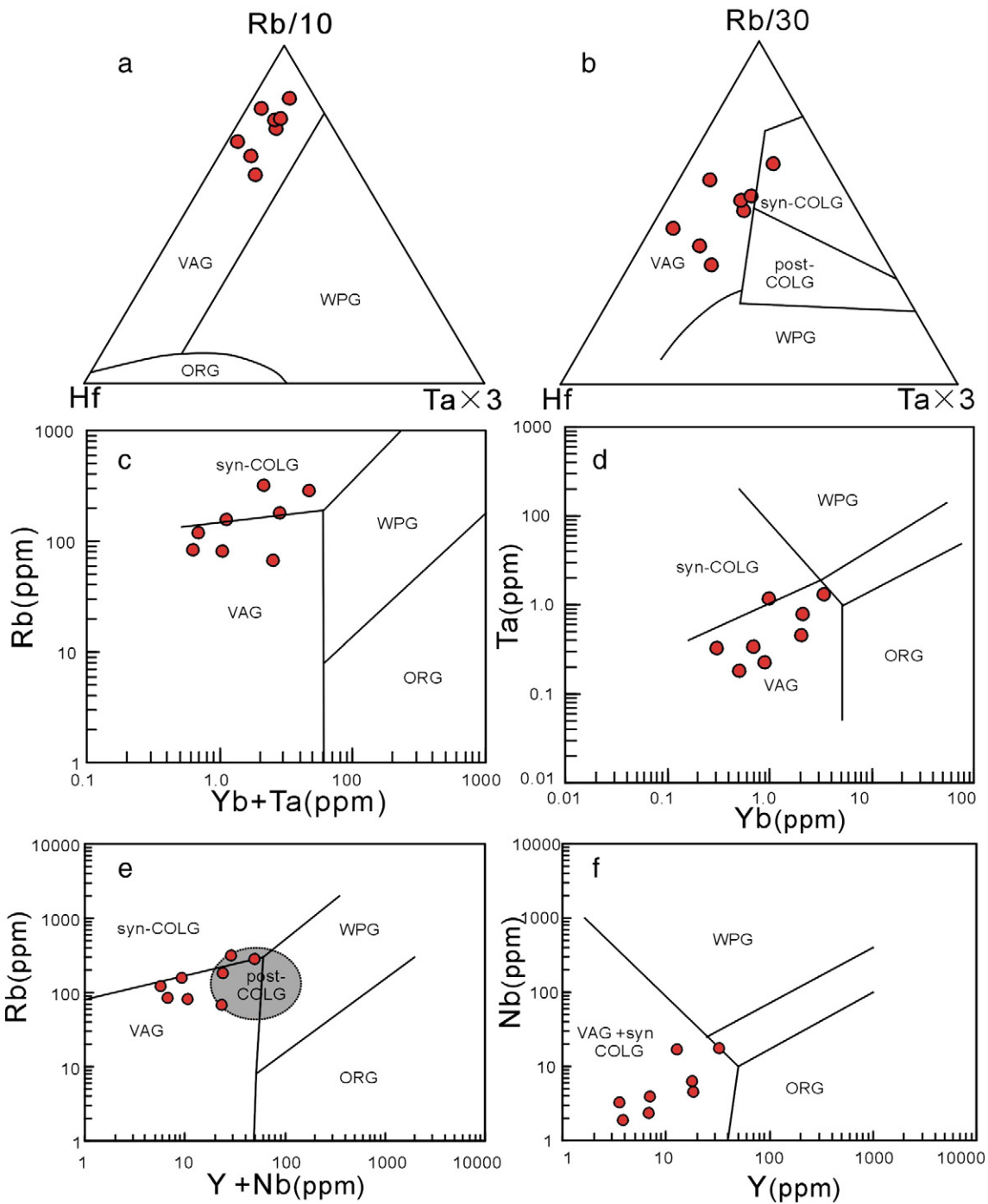


Fig. 13. The discrimination diagrams of tectonic setting. (a) Rb/10-Hf-Ta × 3, and (b) Rb/30-Hf-Ta × 3 (Harris et al., 1986); (c) Rb vs. Yb + Ta, (d) Ta-Yb, (e) Rb vs. Y + Nb and (f) Nb-Y (Pearce et al., 1984) for the early Eocene gneissic granite samples from west Yingjiang. WPG, VAG, syn-COLG, post-COLG and ORG note within-plate granite, volcanic-arc granite, syn-collisional granite, post-collisional granite and ocean-ridge granite, respectively.

7. Conclusion

A comprehensive geochronological and geochemical study on the earliest Eocene I-type gneissic granites in the Nabang metamorphic zone of west Yingjiang (west Yunnan, SW China), a key component of the Mogok metamorphic belt, allows us to reach the following conclusions:

- (1) The gneissic rocks previously-mapped as Precambrian basement in the Nabang metamorphic zone crystallized at the earliest Eocene (50–55 Ma). Their temporal-spatial pattern

and Nd-Hf isotopic compositions resemble those for the Gangdese batholith.

- (2) The gneissic granites from the Nabang metamorphic zone show geochemical characteristics of typical I-type granites. They originated from the crustal materials newly modified by the underplating basaltic magma.
- (3) The Nabang gneissic granites are most likely the equivalent of the Gangdese batholith. Their formation was related to the Neotethyan subduction beneath the Eastern Burma Highlands and Tengchong Block prior to the final collision of India with Eurasia.

Acknowledgements

We wish to acknowledge T-P. Peng, F. Guo, and X-P. Xia, for their help during the fieldwork, and Y. Liu and L Qi and H. Zhang for their assistance during geochemical analyses and LA-ICPMS dating. We are also grateful to Dr. Y-H Zhang for polishing the English. We thank Associate Editor Z-M Zhang and two anonymous reviewers for their critical and constructive review and comments on this paper. This study was jointly supported

by the Natural Science Foundation of China (40830319 and 40825009), “Closed of Eastern Paleotethys Ocean and Assembly of South China continents” (41190073) that is the 3rd research project of a Major NSFC Program (41190070), Most Special Fund from the State Key Laboratory of Continental Dynamics, Northwest University (BJ081331), State Key Laboratory of Ore Deport Geochemistry, CAS (201301) and GIG, CAS (GIGCAS-135-Y234 151001). This is a contribution to Guangzhou Institute of Geochemistry, Chinese Academy of Sciences.

Appendix 1. Zircon U-Pb geochronological analyses of the gneissic granites from the Nabang area in west Yunnan

Spot	Th/U	U-Pb isotopic ratio						Apparent age (Ma)				Hf isotopic ratio				$\epsilon_{\text{Hf}}(t)$	(1 σ)	Model age	
		^{207}Pb	$\pm\%$	^{207}Pb	$\pm\%$	^{206}Pb	$\pm\%$	^{207}Pb	(2 σ)	^{206}Pb	(2 σ)	^{176}Yb	^{176}Lu	^{176}Hf	$\pm\%$				
		^{206}Pb		^{235}U		^{238}U		^{235}U		^{238}U		^{177}Hf	^{177}Hf	^{177}Hf					
<i>DX-66B (Wajiao, N24°42.5', E97°34.754'): Gneissic granites</i>																			
DX-66B-01	0.39	0.0553	6.33	0.0654	7.34	0.0085	1.18	64.3	4.7	54.7	1.2	0.010828	0.000467	0.282899	0.02	5.66	0.79	0.77	0.05
DX-66B-03	0.38	0.0504	1.98	0.0594	2.53	0.0086	2.33	58.6	1.8	55	1.5	0.01436	0.000586	0.282793	0.03	1.93	1.29	1.01	0.08
DX-66B-04	0.46	0.0497	2.82	0.0598	2.84	0.0088	1.14	59	2	56.3	1.3	0.01397	0.000601	0.282796	0.03	2.06	1.32	1	0.08
DX-66B-05	0.49	0.0619	5.65	0.0737	6.38	0.0086	1.16	72.2	4.7	55.1	1.3	0.013024	0.00055	0.282778	0.02	1.41	1.07	1.04	0.07
DX-66B-06	0.51	0.0495	2.22	0.0566	2.3	0.0083	1.2	55.9	1.7	53.6	1.3	0.010852	0.000472	0.28286	0.02	4.26	1.18	0.86	0.08
DX-66B-07	0.4	0.0529	3.21	0.0626	4.31	0.0085	1.18	61.7	2.8	54.8	1.4	0.019291	0.000776	0.282873	0.01	4.76	0.6	0.83	0.04
DX-66B-08	0.63	0.0486	7	0.0575	9.91	0.0085	1.18	56.8	5.6	54.5	1.3	0.011997	0.000511	0.282959	0.01	7.8	0.62	0.63	0.04
DX-66B-09	0.52	0.0508	6.5	0.0608	9.38	0.0086	1.16	60	5.6	54.9	1.3								
DX-66B-10	0.45	0.0592	3.55	0.0693	5.34	0.0083	2.41	68	3.7	53.5	1.7	0.013168	0.000599	0.282861	0.02	4.28	0.95	0.86	0.06
DX-66B-14	0.73	0.0471	2.55	0.0571	2.98	0.0088	1.14	56.4	2	56.3	1.2	0.016043	0.000654	0.282937	0.03	7.06	1.48	0.68	0.1
DX-66B-15	0.35	0.0537	8.19	0.0623	9.63	0.0084	2.38	61.4	5.9	54	1.5	0.007783	0.000366	0.282894	0.01	5.47	0.65	0.78	0.04
DX-66B-17	0.58	0.0472	2.75	0.0556	2.88	0.0086	1.16	55	1.9	54.9	1.3	0.011404	0.000485	0.282912	0.01	6.14	0.59	0.74	0.04
DX-66B-18	0.38	0.0478	1.88	0.0622	3.05	0.0094	2.13	61.3	2.1	60.5	1.9	0.014243	0.000597	0.282726	0.03	-0.34	1.86	1.16	0.1
DX-66B-21	0.39	0.0498	2.01	0.0595	2.52	0.0087	2.3	58.7	1.8	55.8	1.5	0.015322	0.000655	0.282952	0.01	7.56	0.63	0.65	0.04
DX-66B-22	0.28	0.0519	5.01	0.0627	8.93	0.0086	2.33	61.7	5.5	55.3	1.7	0.007314	0.000359	0.282949	0.05	7.47	2.28	0.65	0.15
DX-66B-23	0.54	0.0487	2.26	0.0563	3.55	0.0084	1.19	55.7	2.2	53.9	1.3	0.015158	0.000638	0.282816	0.01	2.72	0.62	0.96	0.04
DX-66B-24	0.5	0.048	3.75	0.0584	3.6	0.0089	1.12	57.7	2.3	57	1.4	0.01741	0.00071	0.282937	0.04	7.07	2.14	0.68	0.14
DX-66B-25	0.34	0.0488	2.05	0.0562	3.2	0.0084	2.38	55.5	2	53.8	1.6	0.011165	0.000495	0.283036	0.01	10.51	0.65	0.46	0.04
DX-66B-26	0.41	0.0483	2.48	0.0606	2.97	0.0091	1.1	59.8	2.1	58.6	1.4	0.018078	0.000764	0.282822	0.01	3.01	0.71	0.94	0.05
DX-66B-29	0.5	0.0485	3.92	0.0585	3.93	0.0088	1.14	57.8	2.5	56.4	1.5	0.014388	0.000572	0.282958	0.01	7.78	0.67	0.63	0.04
<i>DX-66D (Wajiao, N24°42.5', E97°34.754'): Leucogranite</i>																			
DX-66D-02	0.38	0.0487	1.64	0.0546	4.58	0.0081	3.7	54	2.4	52.2	2.2	0.046334	0.002043	0.282914	0.01	6.11	0.67	0.74	0.04
DX-66D-03	0.35	0.0485	2.06	0.0554	2.89	0.0083	2.41	54.8	1.6	53.2	1.2	0.026951	0.001277	0.283055	0.01	11.14	0.69	0.42	0.05
DX-66D-05	0.34	0.0463	0.86	0.0517	1.74	0.0081	1.23	51.2	0.9	52	0.8								
DX-66D-06	0.31	0.0466	0.86	0.0516	1.55	0.008	1.25	51.1	0.7	51.5	0.7	0.076477	0.003431	0.282862	0.01	4.18	0.38	0.86	0.02
DX-66D-08	0.35	0.0467	0.86	0.0523	1.91	0.0081	2.47	51.7	0.9	52.2	1								
DX-66D-09	0.68	0.0471	0.85	0.0534	2.06	0.0082	2.44	52.8	1.1	52.7	1.1	0.036896	0.001636	0.282862	0.01	4.26	0.69	0.86	0.04
DX-66D-11	0.34	0.0482	2.49	0.0551	3.45	0.0083	1.2	54.5	1.8	53	0.7	0.053998	0.002491	0.282996	0.01	8.98	0.74	0.55	0.05
DX-66D-13	0.34	0.0481	1.46	0.0549	2.37	0.0083	2.41	54.3	1.2	53.2	1.1	0.030729	0.001465	0.282943	0.02	7.18	0.92	0.67	0.06
DX-66D-14	0.34	0.0465	0.65	0.0528	1.7	0.0082	1.22	52.2	0.9	52.9	0.9	0.03264	0.001613	0.282941	0.02	7.08	0.78	0.68	0.05
DX-66D-16	0.43	0.048	1.67	0.0553	2.17	0.0084	1.19	54.7	1.1	53.7	0.8	0.041776	0.001937	0.282995	0.01	9.01	0.46	0.55	0.03
DX-66D-18	0.33	0.049	3.88	0.056	4.82	0.0082	1.22	55.3	2.6	53	0.8	0.091331	0.004096	0.28263	0.04	-4.02	1.87	1.38	0.12
DX-66D-19	0.48	0.0486	2.47	0.0549	3.1	0.0082	1.22	54.2	1.6	52.4	0.9	0.088091	0.00397	0.28283	0.01	3.05	0.61	0.93	0.04
DX-66D-20	0.28	0.0535	7.66	0.0602	9.47	0.0081	2.47	59.4	5.4	51.8	1.6	0.041878	0.001924	0.282878	0.02	4.82	0.93	0.82	0.06
DX-66D-21	0.29	0.0467	0.64	0.0531	1.32	0.0082	1.22	52.5	0.7	52.9	0.7	0.036628	0.001665	0.282895	0.03	5.46	1.55	0.78	0.1
DX-66D-22	0.6	0.0458	0.44	0.0531	1.32	0.0084	1.19	52.5	0.6	54	0.7								
DX-66D-24	0.38	0.0471	1.06	0.0537	1.49	0.0083	1.2	53.1	0.7	53.1	0.6	0.058075	0.002529	0.282803	0.02	2.18	0.97	0.99	0.06
DX-66D-25	0.49	0.0467	1.5	0.0525	1.9	0.0081	1.23	51.9	0.9	52.3	0.5	0.065819	0.002966	0.282831	0.01	3.14	0.68	0.93	0.04
<i>DX-59A (Laodaonong, N24°40.382', E97°35.061'): Hornblende-bearing gneissic granites</i>																			
DX-59A-01	0.83	0.0339	20.65	0.0382	20.16	0.0085	3.53	38.1	7.5	54.4	1.6								
DX-59A-02	0.54	0.0485	7.63	0.0569	7.38	0.0086	2.33	56.2	4.1	55.1	1.1								
DX-59A-05	0.62	0.0489	9.41	0.0564	8.87	0.0085	2.35	55.8	4.8	54.8	1.2								
DX-59A-06	0.6	0.0544	9.74	0.0606	9.08	0.0083	2.41	59.7	5.2	53.1	1.4								
DX-59A-07	0.53	0.0691	9.99	0.0784	10.08	0.0083	2.41	76.7	7.5	53.3	1.3								
DX-59A-08	0.08	0.0551	2.9	0.0493	3.83	0.00606	2.97	383.8	12.2	379.5	11.2								
DX-59A-09	0.77	0.0556	9.89	0.0621	9.18	0.0084	2.38	61.2	5.5	53.6	1.3								
DX-59A-10	0.79	0.0516	8.72	0.0628	7.96	0.0091	2.2	61.9	4.8	58.1	1.4								
DX-59A-12	0.47	0.0488	9.43	0.056	8.93	0.009	12.22	55.3	4.8	57.7	7.1								
DX-59A-13	0.51	0.0567	9.52	0.0664	9.34	0.0086	2.33	65.2	5.9	55.3	1.5								
DX-59A-14	0.61	0.0479	13.15	0.0528	13.														

Appendix 1 (continued)

Spot	Th/U	U-Pb isotopic ratio						Apparent age (Ma)				Hf isotopic ratio				$\epsilon_{\text{HF}}(t)$	(1 σ)	Model age																
		$\frac{^{207}\text{Pb}}{^{206}\text{Pb}}$		$\pm\%$		$\frac{^{207}\text{Pb}}{^{235}\text{U}}$		$\pm\%$		$\frac{^{206}\text{Pb}}{^{238}\text{U}}$		$\pm\%$		$\frac{^{207}\text{Pb}}{^{235}\text{U}}$		(2 σ)		$\frac{^{206}\text{Pb}}{^{238}\text{U}}$		(2 σ)		$\frac{^{176}\text{Yb}}{^{177}\text{Hf}}$		$\frac{^{176}\text{Lu}}{^{177}\text{Hf}}$		$\frac{^{176}\text{Hf}}{^{177}\text{Hf}}$		$\pm\%$		$\epsilon_{\text{HF}}(t)$	(1 σ)	Model age		
																														T _{DM}	(1 σ)	(Ga)		
<i>DX-59A (Laodaonong, N24°40.382', E97°35.061'): Hornblende-bearing orthogneiss</i>																																		
DX-59A-24	0.54	0.0498	9.04	0.0585	9.06	0.0086	2.33	57.7	5	55.2	1.2																							
DX-59A-25	0.47	0.0538	10.59	0.0605	10.25	0.0086	5.81	59.7	5.9	54.9	3.3																							
<i>DX-58 (Nankai, N24°38.511', E97°34.967'): Gneissic granites</i>																																		
DX-58A-01	0.63	0.0514	12.45	0.0575	12.35	0.0081	3.7	56.7	6.8	52.1	1.7	0.026397	0.00093	0.282905	0.01	5.81	0.36	0.76	0.02															
DX-58A-02	0.5	0.0528	12.88	0.0563	11.9	0.008	2.5	55.6	6.4	51.1	1.5	0.023926	0.000879	0.282934	0.01	6.83	0.36	0.69	0.02															
DX-58A-03	0.87	0.048	11.67	0.0542	11.25	0.0083	2.41	53.6	5.9	53.1	1.3																							
DX-58A-04	0.65	0.0523	12.62	0.0585	12.48	0.0082	2.44	57.7	7	52.7	1.6	0.024705	0.000865	0.282892	0.01	5.37	0.49	0.79	0.03															
DX-58A-05	0.77	0.048	16.25	0.0504	14.88	0.0079	2.53	50	7.2	50.8	1.5	0.036359	0.001269	0.28278	0.01	1.36	0.47	1.04	0.03															
DX-58A-06	0.74	0.0508	8.86	0.0547	8.96	0.0078	2.56	54.1	4.7	50.4	1.4	0.032437	0.001117	0.2829	0.01	5.59	0.41	0.77	0.03															
DX-58A-07	0.51	0.0472	13.77	0.0501	13.77	0.0078	3.85	49.6	6.7	50.1	1.6	0.033477	0.001196	0.282922	0.01	6.35	0.35	0.72	0.02															
DX-58A-08	0.62	0.0523	10.52	0.0871	10.1	0.0123	2.44	84.8	8.2	78.6	2	0.023699	0.000901	0.282934	0.01	7.41	0.5	0.68	0.03															
DX-58A-09	0.44	0.0469	12.15	0.0504	11.51	0.0079	2.53	50	5.6	50.8	1.4	0.020157	0.000719	0.282881	0.01	4.95	0.41	0.81	0.03															
DX-58A-10	0.64	0.0473	12.9	0.0533	13.13	0.0083	3.61	52.8	6.8	53.2	1.8	0.03709	0.001293	0.282924	0.01	6.48	0.45	0.71	0.03															
DX-58A-11	0.41	0.0512	9.18	0.134	8.43	0.0193	3.11	127.7	10.1	123.2	3.6	0.021877	0.000834	0.282982	0.01	10.06	0.44	0.54	0.03															
DX-58A-12	0.68	0.0469	12.37	0.0527	11.76	0.0083	3.61	52.1	5.9	53.4	1.9	0.025551	0.000934	0.282905	0.01	5.82	0.37	0.76	0.02															
DX-58A-13	0.36	0.0464	4.74	0.0672	4.91	0.0105	1.9	66	3.1	67.2	1.3	0.076759	0.002787	0.282745	0.01	0.38	0.4	1.11	0.03															
DX-58A-14	0.61	0.0466	5.58	0.0492	5.49	0.0077	1.3	48.8	2.6	49.2	0.9	0.052146	0.001865	0.28292	0.01	6.24	0.4	0.73	0.03															
DX-58A-15	1.03	0.0469	8.53	0.0499	8.22	0.0078	2.56	49.4	4	50	1.3	0.043222	0.001517	0.282917	0.01	6.16	0.41	0.73	0.03															
DX-58A-16	0.54	0.0511	8.02	0.0601	8.65	0.0085	2.35	59.3	5	54.4	1.2	0.041087	0.001494	0.282828	0.01	3.11	0.46	0.93	0.03															
DX-58A-17	0.73	0.0577	9.88	0.0588	10.2	0.0074	2.7	58	5.8	47.3	1.1	0.033776	0.001134	0.282899	0.01	5.49	0.59	0.77	0.04															
DX-58A-18	0.86	0.0466	8.37	0.0518	8.49	0.0081	2.47	51.3	4.3	51.8	1	0.050102	0.001751	0.282863	0.01	4.3	0.45	0.85	0.03															
DX-58A-19	0.7	0.0467	9.21	0.0471	9.13	0.0073	2.74	46.7	4.1	47.1	1	0.040419	0.001472	0.282774	0.01	1.04	0.48	1.06	0.03															
DX-58A-20	0.8	0.0462	13.42	0.0468	11.97	0.0076	2.63	46.4	5.4	48.6	1.5	0.047375	0.001645	0.282801	0.01	2.03	0.61	1	0.04															
DX-58A-21	0.53	0.0475	13.89	0.0529	13.61	0.0082	3.36	52.4	7	52.8	2.1	0.030293	0.001073	0.282849	0.01	3.85	0.48	0.88	0.03															
DX-58A-22	0.64	0.0505	7.72	0.2535	8.17	0.0363	2.48	229.4	16.8	230	5.8	0.022603	0.000967	0.282926	0.01	10.37	0.55	0.6	0.04															
DX-58A-23	0.55	0.0462	8.44	0.0532	8.27	0.0084	2.38	52.6	4.3	53.9	1.3	0.029258	0.001037	0.28275	0.01	0.36	0.46	1.11	0.03															
DX-58A-24	0.47	0.047	11.06	0.0507	10.26	0.0079	2.53	50.2	5	51	1.1	0.021064	0.000812	0.282934	0.01	6.81	0.56	0.69	0.04															
DX-58A-25	0.57	0.0465	12.9	0.053	13.4	0.0082	2.44	52.5	6.8	52.9	1.4	0.031639	0.001116	0.282841	0.01	3.57	0.41	0.9	0.03															
<i>DX-57 (Nankai, N24°37.492', E97°34.970'): Gneissic granites</i>																																		
DX-57-01	0.67	0.045	5.56	0.0507	5.52	0.0082	1.22	50.3	2.7	52.7	0.8	0.025195	0.000969	0.282922	0.01	6.42	0.67	0.72	0.04															
DX-57-03	0.63	0.0474	9.07	0.0495	8.89	0.0076	1.32	49	4.3	48.6	0.7	0.036187	0.001416	0.28295	0.01	7.3	0.53	0.66	0.03															
DX-57-04	0.53	0.0475	13.26	0.0531	13.94	0.0081	1.23	52.6	7.1	51.9	0.9	0.031108	0.001157	0.282851	0.01	3.9	0.52	0.88	0.03															
DX-57-05	0.46	0.0472	5.3	0.05	4.4	0.0077	1.3	49.6	2.1	49.7	0.8																							
DX-57-08	0.63	0.0433	5.77	0.0446	5.61	0.0075	1.33	44.3	2.4	48.1	0.7	0.044037	0.001517	0.282686	0.01	-2.04	0.48	1.25	0.03															
DX-57-09	0.43	0.0417	9.59	0.0462	9.09	0.0082	2.44	45.9	4	52.7	1.1	0.031422	0.001171	0.282817	0.01	2.71	0.58	0.96	0.04															
DX-57-10	0.73	0.0476	6.72	0.0495	6.46	0.00																												

Appendix 1 (continued)

Spot	Th/U	U-Pb isotopic ratio						Apparent age (Ma)				Hf isotopic ratio				$\epsilon_{\text{Hf}}(t)$	(1 σ)	Model age	
		$\frac{^{207}\text{Pb}}{^{206}\text{Pb}}$	$\pm\%$	$\frac{^{207}\text{Pb}}{^{235}\text{U}}$	$\pm\%$	$\frac{^{206}\text{Pb}}{^{238}\text{U}}$	$\pm\%$	$\frac{^{207}\text{Pb}}{^{235}\text{U}}$	(2 σ)	$\frac{^{206}\text{Pb}}{^{238}\text{U}}$	(2 σ)	$\frac{^{176}\text{Yb}}{^{177}\text{Hf}}$	$\frac{^{176}\text{Lu}}{^{177}\text{Hf}}$	$\frac{^{176}\text{Hf}}{^{177}\text{Hf}}$	$\pm\%$	T_{DM}	(1 σ)		
<i>DX-56B (Jinzhuzai, N24°36.812', E97°35.153'): Gneissic granites</i>																			
DX-56B-24	0.13	0.0558	3.41	0.5232	3.36	0.0677	1.18	427.3	11.7	422.4	5								
DX-56B-25	0.37	0.0473	10.57	0.0524	10.5	0.008	2.5	51.8	5.3	51.6	1.3								
<i>YJ-2A (Jinzhuzai, N24°36.786', E97°35.163'): Gneissic granites</i>																			
YJ-2A-01	0.2	0.0561	2.85	0.4962	2.94	0.064	1.25	409.1	9.9	399.8	4.9								
YJ-2A-02	0.49	0.0547	3.29	0.4651	3.48	0.0615	1.63	387.8	11.2	384.6	5.8								
YJ-2A-03	0.05	0.056	3.57	0.3453	3.59	0.0446	1.12	301.2	9.3	281.5	3.2								
YJ-2A-04	0.05	0.0566	3	0.4893	3.13	0.0626	1.44	404.4	10.4	391.4	5.3								
YJ-2A-05	0.44	0.0566	3.71	0.395	4.68	0.0506	3.36	338	13.5	318.4	10.2								
YJ-2A-06	0.84	0.0559	3.22	0.3949	4.89	0.051	3.53	337.9	14.1	320.6	11								
YJ-2A-07	0.82	0.0649	6.32	0.0774	6.33	0.0087	1.15	75.7	4.6	55.6	0.9								
YJ-2A-08	0.17	0.0549	3.28	0.516	3.26	0.0681	1.17	422.5	11.3	424.7	5.1								
YJ-2A-09	0.08	0.0567	3.35	0.5008	3.73	0.0641	1.87	412.2	12.7	400.4	7.5								
YJ-2A-10	0.44	0.0516	7.17	0.0583	7.03	0.0083	2.41	57.6	4	53.1	1								
YJ-2A-11	0.46	0.057	4.39	0.5317	4.4	0.0676	1.33	432.9	15.5	421.8	5.6								
YJ-2A-12	0.28	0.0548	3.65	0.514	3.83	0.0679	1.77	421.1	13.2	423.6	7.2								
YJ-2A-13	0.07	0.0561	3.21	0.5262	3.21	0.0678	1.18	429.3	11.2	422.9	4.7								
YJ-2A-14	0.75	0.0564	4.08	0.5344	3.91	0.0686	1.31	434.7	13.8	428	5.1								
YJ-2A-15	0.14	0.0554	4.15	0.5177	3.96	0.0677	1.62	423.6	13.7	422.4	6.5								
YJ-2A-16	0.62	0.0538	8.36	0.0619	8.72	0.0083	2.41	61	5.2	53.5	1.3								
YJ-2A-17	0.28	0.0539	4.08	0.51	3.96	0.0684	1.17	418.5	13.6	426.7	5								
YJ-2A-18	0.11	0.0556	4.14	0.521	4.15	0.0676	1.33	425.8	14.4	421.8	5.6								
YJ-2A-19	0.11	0.0541	3.33	0.4785	3.28	0.064	1.25	397	10.8	399.7	4.9								
YJ-2A-20	0.54	0.0483	6.63	0.0534	6.93	0.008	2.5	52.8	3.6	51.5	1								
YJ-2A-21	0.27	0.0556	4.5	0.5174	4.68	0.0674	2.08	423.4	16.2	420.7	8.6								
YJ-2A-22	0.11	0.0551	3.27	0.5174	3.38	0.0678	1.62	423.4	11.7	423.2	6.4								
YJ-2A-23	0.08	0.0557	4.13	0.5219	4.02	0.0678	1.47	426.4	14	422.7	5.8								
YJ-2A-24	0.96	0.0543	3.68	0.5095	3.67	0.0677	1.18	418.1	12.6	422.2	5								
YJ-2A-25	0.13	0.0559	3.94	0.5228	3.88	0.0674	1.48	427	13.5	420.8	5.8								
<i>DX-53C (Tongbiguan, N24°37.048', E97°38.389'): Leucogranite</i>																			
DX-53C-01	0.18	0.0472	0.42	0.0533	0.94	0.0082	1.22	52.7	0.5	52.5	0.4	0.00001	0.002257	0.282456	0.02	-10.09	0.93	1.76	0.06
DX-53C-02	0.18	0.0473	0.63	0.0542	1.29	0.0083	1.2	53.6	0.7	53.3	0.6	0.000183	0.003624	0.282507	0.02	-8.33	0.74	1.65	0.05
DX-53C-03	0.2	0.0473	0.63	0.0542	1.29	0.0083	1.2	53.6	0.7	53.3	0.6	0.000047	0.002021	0.282584	0.01	-5.54	0.73	1.48	0.05
DX-53C-04	0.22	0.0475	0.63	0.0545	1.1	0.0083	1.2	53.9	0.6	53.5	0.5								
DX-53C-05	0.13	0.0474	0.84	0.0543	1.29	0.0083	1.2	53.7	0.7	53.4	0.6	0.000121	0.002263	0.282643	0.01	-3.48	0.52	1.35	0.03
DX-53C-06	0.17	0.0473	0.63	0.0539	0.93	0.0083	1.2	53.3	0.5	53.1	0.4	0.000063	0.002814	0.282644	0.01	-3.47	0.5	1.35	0.03
DX-53C-07	0.16	0.047	0.85	0.0547	1.46	0.0084	1.19	54.1	0.7	54.2	0.6	0.000112	0.002301	0.282621	0.02	-4.24	1.06	1.4	0.07
DX-53C-08	0.18	0.0466	0.43	0.0533	1.31	0.0083	1.2	52.8	0.6	53.3	0.6	0.000025	0.002721	0.282576	0.01	-5.88	0.54	1.5	0.03
DX-53C-09	0.13	0.0464	0.86	0.0538	1.67	0.0084	1.19	53.2	0.8	54	0.8	0.000021	0.001556	0.282627	0.03	-3.99	1.57	1.38	0.1
DX-53C-10	0.28	0.0465	0.86	0.0538	1.49	0.0084	1.19	53.2	0.8	53.9	0.7	0.000067	0.003	0.282659	0.01	-2.93	0.53	1.31	0.03
DX-53C-11	0.2	0.0475	0.63	0.0533	0.94	0.0082	1.22	52.7	0.5	52.3	0.4	0.000046	0.002282	0.282616	0.04	-4.46	2	1.41	0.13
DX-53C-12	0.15	0.0473	0.85	0.0542	1.11	0.0083	1.2	53.6	0.6	53.3	0.5								
DX-53C-13	0.22	0.0467	0.43	0.0536	0.93	0.0083	1.2	53	0.5	53.5	0.5	0.000092	0.003734	0.282454	0.02	-10.22	0.95	1.77	0.06
DX-53C-14	0.22	0.0474	0.42	0.0538	1.12	0.0082	1.22	53.2	0.6	52.8	0.6	0.000127	0.001998	0.282482	0.03	-9.18	1.28	1.71	0.08
DX-53C-15	0.13	0.0477	0.63	0.054	1.3	0.0082	1.22	53.4	0.6	52.8	0.6	0.000128	0.002061	0.282638	0.01	-3.65	0.67	1.36	0.04
DX-53C-16	0.2	0.0476	1.26	0.0541	1.66	0.0082	1.22	53.5	0.9	52.9	0.6	0.000121	0.001587	0.282603	0.01	-4.87	0.68	1.44	0.04
DX-53C-17	0.2	0.0476	0.63	0.0538	1.12	0.0082	1.22	53.2	0.6	52.6	0.5								
DX-53C-18	0.15	0.0477	0.63	0.0538	1.12	0.0082	1.22	53.2	0.6	52.5	0.5	0.000047	0.00221	0.282578	0.01	-5.77	0.4	1.49	0.03
DX-53C-19	0.21	0.0473	0.42	0.0533	1.31	0.0082	1.22	52.8	0.7	52.5	0.7	0.000083	0.003414	0.282516	0.02	-8.02	1.05	1.63	0.07
DX-53C-20	0.19	0.0486	0.82	0.0545	2.02	0.0082	1.22	53.9	1.1	52.5	0.9	0.000071	0.002138	0.282499	0.02	-8.56	0.9	1.67	0.06
DX-53C-21	0.23	0.0481	0.42	0.0541	0.92	0.0082	1.22	53.5	0.5	52.4	0.4	0.000102	0.004208	0.282625	0.01	-4.18	0.72	1.39	0.05
DX-53C-22	0.14	0.0486	0.62	0.0552	1.09	0.0082	1.22	54.5	0.6	52.8	0.5	0.00007	0.001995	0.282672	0.01	-2.45	0.68	1.28	0.04
DX-53C-23	0.18	0.0476	0.63	0.0545	0.92	0.0083	1.2	53.9	0.5	53.2	0.4	0.000022	0.002562	0.28265	0.02	-3.25	0.82	1.33	0.05
DX-53C-24	0.12	0.0476	0.63	0.0542	1.11	0.0083	1.2	53.6	0.6	53.2	0.6	0.000043	0.001664	0.282693	0.01	-1.68	0.7	1.23	0.05
DX-53C-25	0.2	0.0469	0.43	0.0539	0.93	0.0083	1.2	53.3	0.5	53.5	0.4	0.000059	0.002612	0.282676	0.02	-2.32	0.77	1.28	0.05
DX-53C-26	0.16	0.0473	0.63	0.0544	1.29	0.0083	1.2	53.8	0.7	53.5	0.6	0.000073	0.001624	0.282681	0.02	-2.1	0.74	1.26	0.05
DX-53C-27	0.16	0.0508	1.38	0.058	2.41	0.0082	1.22	57.2	1.3	52.9	0.6								
DX-53C-28	0.23	0.0467	0.43	0.0537	0.93	0.0083	1.2	53											

Appendix 1 (continued)

Spot	Th/U	U-Pb isotopic ratio						Apparent age (Ma)				Hf isotopic ratio				$\epsilon_{\text{Hf}}(t)$	(1 σ)	Model age	
		$\frac{^{207}\text{Pb}}{^{206}\text{Pb}}$	±%	$\frac{^{207}\text{Pb}}{^{235}\text{U}}$	±%	$\frac{^{206}\text{Pb}}{^{238}\text{U}}$	±%	$\frac{^{207}\text{Pb}}{^{235}\text{U}}$	(2 σ)	$\frac{^{206}\text{Pb}}{^{238}\text{U}}$	(2 σ)	$\frac{^{176}\text{Yb}}{^{177}\text{Hf}}$	$\frac{^{176}\text{Lu}}{^{177}\text{Hf}}$	$\frac{^{176}\text{Hf}}{^{177}\text{Hf}}$	±%	T _{DM}	(1 σ)		
																	(Ga)		
DX-67 (Tongbiguan, N24°35.074', E97°41.139'): Gneissic granites																			
DX-67-13	0.64	0.0661	2.42	0.6487	2.42	0.0718	2.51	507.7	9.7	447.2	10.9	0.034336	0.001282	0.282426	0.01	-2.78	0.52	1.61	0.03
DX-67-15	0.61	0.0528	3.98	0.0575	4	0.0079	2.53	56.8	2.2	51	1.2	0.077088	0.002981	0.282554	0.01	-6.68	0.66	1.55	0.04
DX-67-17	0.64	0.0514	3.7	0.0568	3.7	0.008	2.5	56.1	2	51.6	1.3	0.026487	0.000991	0.282685	0.01	-1.99	0.45	1.25	0.03
DX-67-19	0.21	0.054	2.41	0.0621	2.42	0.0084	2.38	61.2	1.4	53.6	1.2	0.039295	0.001495	0.282586	0.01	-5.44	0.4	1.47	0.03
DX-67-20	0.43	0.0561	4.81	0.069	5.65	0.0089	2.25	67.7	3.7	56.9	1.4	0.014546	0.00062	0.282687	0.01	-1.77	0.38	1.24	0.02
DX-67-21	0.92	0.0493	2.64	0.0559	3.04	0.0082	2.44	55.2	1.7	52.8	1.3	0.032408	0.001193	0.282573	0.01	-5.94	0.47	1.5	0.03
DX-67-22	0.46	0.0499	2.2	0.0529	2.27	0.0077	2.6	52.3	1.1	49.4	1.1	0.077088	0.002981	0.282554	0.01	-6.72	0.66	1.55	0.04
DX-67-25	0.74	0.0514	2.92	0.0617	5.35	0.0087	4.6	60.7	3.1	55.7	2.6	0.034306	0.001268	0.282633	0.01	-3.74	0.49	1.37	0.03

Notes: $^{176}\text{Hf}/^{177}\text{Hf}(t) = (\frac{^{176}\text{Lu}}{^{177}\text{Hf}})_{\text{sample}} - (\frac{^{176}\text{Hf}}{^{177}\text{Hf}})_{\text{sample}} \times (e^{\lambda t} - 1)$, $\lambda_{\text{Lu-Hf}} = 0.001865 \text{ Ga}^{-1}$. $\epsilon_{\text{Hf}}(t) = [(\frac{^{176}\text{Hf}}{^{177}\text{Hf}})_{\text{sample}}(t)/(\frac{^{176}\text{Lu}}{^{177}\text{Hf}})_{\text{CHUR}}(t) - 1] \times 10^4$, $(\frac{^{176}\text{Lu}}{^{177}\text{Hf}})_{\text{CHUR}}(t) = 0.282772 - 0.0332 \times (e^{\lambda t} - 1)$.

Appendix 2. Elemental analytical results for the gneissic granites in the Nabang area from west Yunnan.

Sample	DX-66A	DX-66B	DX-66C	DX-66D	DX-66F	DX-59A	DX-57	DX-67
(wt%)								
SiO ₂	66.87	66.79	68.63	75.71	73.78	62.71	70.73	73.27
TiO ₂	0.36	0.42	0.34	0.06	0.1	0.56	0.22	0.24
Al ₂ O ₃	15.8	15.58	16.79	12.97	14.18	16.52	14.44	13.53
MgO	1.4	1.56	0.94	0.14	0.3	2.38	0.58	0.3
FeOt	4.72	4.11	2.28	0.98	1.01	5.63	2.57	1.57
CaO	4.41	3.69	3.38	1.11	1.09	5.11	1.31	1.05
K ₂ O	1.62	3.46	2.21	3.99	4.87	2.46	7.4	5.74
Na ₂ O	3.01	3.24	4.38	3.57	3.74	3.26	1.75	2.59
P ₂ O ₅	0.15	0.12	0.12	0.02	0.04	0.14	0.1	0.05
MnO	0.05	0.08	0.04	0.03	0.04	0.1	0.03	0.03
LOI	1.17	0.5	0.43	0.96	0.39	0.57	0.31	0.78
Total	99.55	99.53	99.54	99.55	99.53	99.44	99.44	99.45
A/CNK	1.07	0.99	1.07	1.06	1.06	0.95	1.09	1.09
A/NK	2.36	1.72	1.75	1.27	1.24	2.06	1.33	1.29
(ppm)								
Rb	83.1	179	80.4	118	316	66.8	156	281
Ba	203	360	400	674	100	450	1960	617
Th	8.36	21	11.5	11.7	9.11	7.183	38.9	32.2
U	1.04	4.61	4.5	1.84	6.77	1.687	3.41	5.42
Nb	3.26	6.22	3.83	1.88	16.4	4.452	2.35	17.3
Ta	0.33	0.76	0.33	0.18	1.17	0.45	0.22	1.29
Sr	327	306	670	170	79.9	387.3	453	145
Zr	43.8	83.8	91.3	54.7	39	92.1	236	184
Hf	1.42	2.69	2.95	2.16	2.36	2.854	5.63	5.3
Y	3.63	18.3	7.02	3.86	13	18.81	6.96	32.9
La	16.8	27.9	20.9	17.3	8.33	20.69	98.7	69.6
Ce	33.6	56.9	41.3	32	19.8	41.44	154	139
Pr	2.97	5.82	4.11	2.96	2.28	5.16	14.4	14.5
Nd	9.48	20.1	14.3	9.05	8.78	20.3	42.4	49.3
Sm	1.5	4.03	2.4	1.45	2.49	4.03	4.37	8.36
Eu	0.4	0.7	0.61	0.39	0.24	0.95	0.76	0.9
Gd	1.14	3.38	1.81	1.07	3.01	3.82	3.01	6.66
Tb	0.16	0.55	0.26	0.14	0.49	0.61	0.32	1.03
Dy	0.63	3.05	1.26	0.65	2.44	3.62	1.57	5.32
Ho	0.12	0.71	0.26	0.13	0.48	0.77	0.29	1.22
Er	0.31	1.91	0.69	0.4	1.13	2.18	0.85	3.42
Tm	0.04	0.3	0.1	0.07	0.16	0.31	0.12	0.48
Yb	0.31	2.12	0.72	0.52	1	2.08	0.91	3.43
Lu	0.05	0.29	0.11	0.1	0.13	0.33	0.17	0.51
¹⁴⁷ Sm/ ¹⁴⁴ Nd	0.096	0.121	0.101	0.097	0.172	0.12	0.062	
⁸⁷ Rb/ ⁸⁶ Sr	0.735	1.692	0.347	2.008	11.445	0.513	0.996	
¹⁴³ Nd/ ¹⁴⁴ Nd	0.512666	0.512614	0.512437	0.512663	0.512273	0.512574	0.51249	
(2 σ)	8	10	10	8	12	8	8	
⁸⁷ Sr/ ⁸⁶ Sr	0.705419	0.706213	0.707089	0.706974	0.709353	0.70565	0.706759	
(2 σ)	12	12	12	12	12	16	14	
⁸⁷ Sr/ ⁸⁶ Sr(t)	0.7052	0.7049	0.707	0.7056	0.7061	0.7053	0.706	
$\epsilon_{\text{Nd}}(t)$	0.8	0.1	-3.9	1.1	-7	-0.8	-2	

A/CNK: molar Al₂O₃/(CaO + Na₂O + K₂O). A/NK: molar Al₂O₃/(Na₂O + K₂O).

$^{87}\text{Sr}/^{86}\text{Sr}(t) = \frac{^{87}\text{Sr}}{^{86}\text{Sr}} - (\frac{^{87}\text{Rb}}{^{86}\text{Sr}}) \times (e^{\lambda t} - 1)$, $\lambda_{\text{Rb-Sr}} = 0.0142 \text{ Ga}^{-1}$, $^{87}\text{Rb}/^{86}\text{Sr} = (\text{Rb/Sr}) \times 2.8956$.

$\epsilon_{\text{Nd}}(t) = [(\frac{^{143}\text{Nd}}{^{144}\text{Nd}})_{\text{sample}}(t)/(\frac{^{143}\text{Nd}}{^{144}\text{Nd}})_{\text{CHUR}}(t) - 1] \times 10^4$, $(\frac{^{143}\text{Nd}}{^{144}\text{Nd}})_{\text{CHUR}}(t) = 0.512638 - 0.1967 \times (e^{\lambda t} - 1)$, $\lambda_{\text{Sm-Nd}} = 0.01865 \text{ Ga}^{-1}$, $^{147}\text{Sm}/^{144}\text{Nd} = (\text{Sm/Nd}) \times 0.60456$.

Appendix A. Supplementary data

Supplementary data associated with this article can be found in the online version, at <http://dx.doi.org/10.1016/j.gr.2013.04.010>. These data include Google map of the most important areas described in this article.

References

- Aitchison, J.C., Davis, A.M., 2001. When did the India–Asia collision really happen? *Gondwana Research* 4, 560.
- Aitchison, J.C., Abrajevitch, A., Ali, J.R., Badengzhu Davis, A.M., Luo, H., Liu, J.B., McDermid, I.R.C., Ziabrev, S., 2002. New insights into the evolution of the Yarlung Tsangpo suture zone, Xizang(Tibet), China. *Episodes* 25, 90–94.
- Aitchison, J.C., Ali, J.R., Davis, A.M., 2007. When and where did India and Asia collide? *Journal of Geophysical Research* 112, B05423.
- Aitchison, J.C., Ali, J.R., Davis, A.M., 2008. Reply to comment by Eduardo Garzanti on “When and where did India and Asia collide?”. *Journal of Geophysical Research* 113, B04412.
- Allegre, C., Courtillot, V., Tapponnier, P., Hirn, A., Mattauer, M., Coulon, C., Jaeger, J., Achache, J., Schärer, U., Marcoux, J., 1984. Structure and evolution of the Himalaya-Tibet orogenic belt. *Nature* 307, 17–22.
- Altherr, R., Holl, A., Hegner, E., Langer, C., Kreuzer, H., 2000. High-potassium, calc-alkaline I-type plutonism in the European Variscides: northern Vosges (France) and northern Schwarzwald (Germany). *Lithos* 50, 51–73.
- Anthony, E.Y., 2005. Source regions of granites and their links to tectonic environment: examples from the western United States. *Lithos* 80, 61–74.
- Barley, M., Pickard, A., Zaw, K., Rak, P., Doyle, M., 2003. Jurassic to Miocene magmatism and metamorphism in the Mogok metamorphic belt and the India–Eurasia collision in Myanmar. *Tectonics* 22, 1019.
- Barth, A.P., Wooden, J., Tosdal, R., Morrison, J., 1995. Crustal contamination in the petrogenesis of a calc-alkaline rock series: Josephine Mountain intrusion, California. *Geological Society of America Bulletin* 107, 201–212.
- Bertrand, G., Rangin, C., Maluski, H., Han, T.A., Thein, M., Myint, O., Maw, W., Lwin, S., 1999. Cenozoic metamorphism along the Shan Scarp (Myanmar): evidences for ductile shear along the Sagaing Fault or the northward migration of the Eastern Himalayan Syntaxis? *Geophysical Research Letters* 26, 915–918.
- Bertrand, G., Rangin, C., Maluski, H., Bellon, H., Party, G.S., 2001. Diachronous cooling along the Mogok Metamorphic Belt (Shan scarp, Myanmar): the trace of the northward migration of the Indian syntaxis. *Journal of Asian Earth Sciences* 19, 649–659.
- Blichert-Toft, J., Albarède, F., 1997. The Lu-Hf isotope geochemistry of chondrites and the evolution of the mantle–crust system. *Earth and Planetary Science Letters* 148, 243–258.
- Bottazzi, P., Tiepolo, M., Vannucci, R., Zanetti, A., Brumm, R., Foley, S., Oberti, R., 1999. Distinct site preferences for heavy and light REE in amphibole and the prediction of Amph/L D REE. *Contributions to Mineralogy and Petrology* 137, 36–45.
- Burtman, V., 1994. Meso-Tethyan oceanic sutures and their deformation. *Tectonophysics* 234, 305–327.
- Cai, F., Ding, L., Yue, Y., 2011. Provenance analysis of upper Cretaceous strata in the Tethys Himalaya, southern Tibet: implications for timing of India–Asia collision. *Earth and Planetary Science Letters* 305, 195–206.
- Chappell, B.W., White, A.J.R., 1974. Two contrasting granite types. *Pacific Geology* 8, 173–174.
- Chappell, B.W., White, A.J.R., 2001. Two contrasting granite types: 25 years later. *Australian Journal of Earth Sciences* 48, 489–499.
- Chatterjee, S., Goswami, A., Scotese, C.R., 2013. The longest voyage: tectonic, magmatic, and paleoclimate evolution of the Indian plate during its northward flight from Gondwana to Asia. *Gondwana Research* 23, 238–267.
- Chen, F.K., Li, Q.L., Wang, X.L., Li, X.H., 2006. Zircon age and Sr-Nd-Hf isotopic composition of migmatite in the eastern Tengchong block, western Yunnan. *Acta Petrologica Sinica* 22, 439–448.
- Chen, F.K., Li, X.H., Wang, X.L., Li, Q.L., Siebel, W., 2007. Zircon age and Nd-Hf isotopic composition of the Yunnan Tethyan belt, southwestern China. *International Journal of Earth Sciences* 96, 1179–1194.
- Chiu, H.Y., Chung, S.L., Wu, F.Y., Liu, D., Liang, Y.H., Lin, I.J., Iizuka, Y., Xie, L.W., Wang, Y., Chu, M.F., 2009. Zircon U-Pb and Hf isotopic constraints from eastern Transhimalayan batholiths on the precollisional magmatic and tectonic evolution in southern Tibet. *Tectonophysics* 477, 3–19.
- Chu, M.F., Chung, S.L., Song, B., Liu, D., O'Reilly, S.Y., Pearson, N.J., Ji, J., Wen, D.J., 2006. Zircon U-Pb and Hf isotope constraints on the Mesozoic tectonics and crustal evolution of southern Tibet. *Geology* 34, 745–748.
- Chung, S.L., Chu, M.F., Zhang, Y., Xie, Y., Lo, C.H., Lee, T.Y., Lan, C.Y., Li, X., Zhang, Q., Wang, Y., 2005. Tibetan tectonic evolution inferred from spatial and temporal variations in post-collisional magmatism. *Earth-Science Reviews* 68, 173–196.
- Cobbing, E., Mallick, D., Pitfield, P., Teoh, L., 1986. The granites of the Southeast Asian tin belt. *Journal of the Geological Society* 143, 537–550.
- Debon, F., Le Fort, P., Sheppard, S.M.F., Sonet, J., 1986. The four plutonic belts of the Transhimalaya–Himalaya: a chemical, mineralogical, isotopic, and chronological synthesis along a Tibet–Nepal section. *Journal of Petrology* 27, 219–250.
- Dewey, J.F., Shackleton, R.M., Chengfa, C., Yiyin, S., 1988. The tectonic evolution of the Tibetan Plateau. *Philosophical Transactions of the Royal Society of London. Series A: Mathematical and Physical Sciences* 327, 379–413.
- Ding, L., Zhong, D., 1999. Metamorphic characteristics and geotectonic implications of the high-pressure granulites from Namche Barwa, eastern Tibet. *Science in China Series D: Earth Sciences* 42, 491–505.
- Ding, L., Zhong, D., Yin, A., Kapp, P., Harrison, T.M., 2001. Cenozoic structural and metamorphic evolution of the eastern Himalayan syntaxis (Namche Barwa). *Earth and Planetary Science Letters* 192, 423–438.
- Ding, L., Kapp, P., Wan, X., 2005. Paleocene–Eocene record of ophiolite obduction and initial India–Asia collision, south central Tibet. *Tectonics* 24, TC3001.
- Douce, A.E.P., 1999. What do experiments tell us about the relative contributions of crust and mantle to the origin of granitic magmas? *Geological Society, London, Special Publications* 168, 55–75.
- Douce, A.E.P., Harris, N., 1998. Experimental constraints on Himalayan anatexis. *Journal of Petrology* 39, 689–710.
- Ducea, M., 2001. The California arc: thick granitic batholiths, eclogitic residues, lithospheric-scale thrusting, and magmatic flare-ups. *GSA Today* 11, 4–10.
- Frey, F.A., Chappell, B.W., Roy, S.D., 1978. Fractionation of rare-earth elements in the Tuolumne Intrusive Series, Sierra Nevada batholith, California. *Geology* 6, 239–242.
- Gao, Y.F., Wei, R.H., Hou, Z.Q., Tian, S.H., Zhao, R.S., 2008. Eocene high-MgO volcanism in southern Tibet: new constraints for mantle source characteristics and deep processes. *Lithos* 105, 63–72.
- Garzanti, E., 2008. Comment on “When and where did India and Asia collide?” by Jonathan C. Aitchison, Jason R. Ali, and Aileen M. Davis. *Journal of Geophysical Research* 113, B004412.
- Garzanti, E., Baud, A., Mascle, G., 1987. Sedimentary record of the northward flight of India and its collision with Eurasia (Ladakh Himalaya, India). *Geodinamica Acta* 1, 297–312.
- Gaudemer, Y., Jaupart, C., Tapponnier, P., 1988. Thermal control on post-orogenic extension in collision belts. *Earth and Planetary Science Letters* 89, 48–62.
- Griffin, W.L., Pearson, N.J., Belousova, E., Jackson, S.E., Van Achterbergh, E., O'Reilly, S.Y., Shee, S.R., 2000. The Hf isotope composition of cratonic mantle: LAM-ICPMS analysis of zircon megacrysts in kimberlites. *Geochimica et Cosmochimica Acta* 64, 133–147.
- Guan, Q., Zhu, D.C., Zhao, Z.D., Dong, G.C., Zhang, L.L., Li, X.W., Liu, M., Mo, X.X., Liu, Y.S., Yuan, H.L., 2012. Crustal thickening prior to 38 Ma in southern Tibet: evidence from lower crust-derived adakitic magmatism in the Ganges Batholith. *Gondwana Research* 21, 88–99.
- Guillot, S., Garzanti, E., Baratoux, D., Marquer, D., Mahéo, G., De Sigoyer, J., 2003. Reconstructing the total shortening history of the NW Himalaya. *Geochemistry, Geophysics, Geosystems* 4, 1064.
- Guo, L., Zhang, H.F., Harris, N., Parrish, R., Xu, W.C., Shi, Z.L., 2012. Paleogene crustal anatexis and metamorphism in Lhasa terrane, eastern Himalayan syntaxis: evidence from U-Pb zircon ages and Hf isotopic compositions of the Nyingchi Complex. *Gondwana Research* 21, 100–111.
- Harris, N.B.W., Pearce, J.A., Tindle, A.G., 1986. Geochemical characteristics of collision-zone magmatism. *Geological Society, London, Special Publications* 19, 67–81.
- Harris, N.B.W., Ronghua, X., Lewis, C., Chengwei, J., 1988a. Plutonic rocks of the 1985 Tibet geotraverse, Lhasa to Golmud. *Philosophical Transactions of the Royal Society of London. Series A: Mathematical and Physical Sciences* 327, 145–168.
- Harris, N.B.W., Ronghua, X., Lewis, C.I., Hawkesworth, C., Yuquan, Z., 1988b. Isotope geochemistry of the 1985 Tibet geotraverse, Lhasa to Golmud. *Philosophical Transactions of the Royal Society of London. Series A: Mathematical and Physical Sciences* 263–285.
- Harris, N., Inger, S., Ronghua, X., 1990. Cretaceous plutonism in Central Tibet: an example of post-collision magmatism? *Journal of Volcanology and Geothermal Research* 44, 21–32.
- Healy, B., Collins, W., Richards, S., 2004. A hybrid origin for Lachlan S-type granites: the Murrumbidgee Batholith example. *Lithos* 78, 197–216.
- Hodges, K.V., 2000. Tectonics of the Himalaya and southern Tibet from two perspectives. *Geological Society of America Bulletin* 112, 324–350.
- Hu, X., Sinclair, H.D., Wang, J., Jiang, H., Wu, F., 2012. Late Cretaceous–Palaeogene stratigraphic and basin evolution in the Zhepure Mountain of southern Tibet: implications for the timing of India–Asia initial collision. *Basin Research* 24, 520–543.
- Huang, Y., Zhao, Z.D., Zhang, F.Q., Zhu, D.C., Dong, G.C., Mo, X.X., 2010. Geochemistry and implication of the Gangdese batholiths from Renbu and Lhasa areas in southern Gangdese, Tibet. *Acta Petrologica Sinica* 26, 3131–3142 (in Chinese with English abstract).
- Huang, Y., Zhu, D.C., Zhao, Z.D., Zhang, L.L., Depaolo, D., Hu, Z.C., Yuan, H.L., Mo, X.X., 2012. Petrogenesis and implication of the andesites at 113 Ma in the Nagqu region in northern Lhasa subterrane. *Acta Petrologica Sinica* 28, 1603–1614 (in Chinese with English abstract).
- Hughes, R.W., Galibert, O., Bosshart, G., Ward, F., Oo, T., Smith, M., Sun, T.T., Harlow, G.E., 2000. Burmese jade: the inscrutable gem. *Gems & Gemology* 36, 2–25.
- Jaeger, J.J., Courtillot, V., Tapponnier, P., 1989. Paleontological view of the ages of the Deccan Traps, the Cretaceous/Tertiary boundary, and the India–Asia collision. *Geology* 17, 316–319.
- Ji, J.Q., Zhong, D.L., Lin, D., Xiuling, H., 1998. Study on metamorphism of granulite facies metamorphic rocks discovered in the Nabang area on the border between China and Burma. *Acta Petrologica Sinica* 14, 163–175 (in Chinese with English abstract).
- Ji, J.Q., Zhong, D.L., Shang, H.Q., Qiu, J., Hu, S.L., 2000a. Dating of two metamorphic events on the basalt granulite from the Nabang area on the border of China and Burma. *Acta Petrologica Sinica* 16, 227 (in Chinese with English abstract).
- Ji, J.Q., Zhong, D.L., Chen, C.Y., 2000b. Geochemistry and genesis of Nabang metamorphic basalt, southwest Yunnan, China: implications for the subducted slab break-off. *Acta Petrologica Sinica* 16, 433–442 (in Chinese with English abstract).
- Ji, J.Q., Zhong, D.L., Zhang, L.S., 2000c. Kinematics and dating of Cenozoic strike-slip faults in the Tengchong area, West Yunnan: implications for the block movement in the southeastern Tibet plateau. *Scientia Geologica Sinica* 35, 336–349 (in Chinese with English abstract).

- Ji, W.Q., Wu, F.Y., Chung, S.L., Li, J.X., Liu, C.Z., 2009. Zircon U-Pb geochronology and Hf isotopic constraints on petrogenesis of the Gangdese batholith, southern Tibet. *Chemical Geology* 262, 229–245.
- Ji, W.Q., Wu, F.Y., Liu, C.Z., Chung, S.L., 2012. Early Eocene crustal thickening in southern Tibet: new age and geochemical constraints from the Gangdese batholith. *Journal of Asian Earth Sciences* 53, 82–95.
- Jiang, W., Mo, X., Zhao, C., Guo, T., Zhang, S., 1999. Geochemistry of granitoid and its mafic microgranular enclave in Gangdese belt, Qinghai-Xizang Plateau. *Acta Petrologica Sinica* 15, 89–97.
- Kapp, J.L.D.A., Harrison, T.M., Kapp, P., Grove, M., Lovera, O.M., Lin, D., 2005. Nyainqntanglha Shan: a window into the tectonic, thermal, and geochemical evolution of the Lhasa block, southern Tibet. *Journal of Geophysical Research* 110, B08413.
- Klein, M., Stosch, H.G., Seck, H.A., 1997. Partitioning of high field-strength and rare-earth elements between amphibole and quartz-dioritic to tonalitic melts: an experimental study. *Chemical Geology* 138, 257–271.
- Klootwijk, C.T., Gee, J.S., Pearce, J.W., Smith, G.M., McFadden, P.L., 1992. An early India-Asia contact: paleomagnetic constraints from Ninetyeast Ridge, ODP Leg 121. *Geology* 20, 395–398.
- Kohn, M.J., Parkinson, C.D., 2002. Petrologic case for Eocene slab breakoff during the Indo-Asian collision. *Geology* 30, 591–594.
- Lee, H.Y., Chung, S.L., Wang, J.R., Wen, D.J., Lo, C.H., Yang, T.F., Zhang, Y., Xie, Y., Lee, T.Y., Wu, G., 2003. Miocene Jiali faulting and its implications for Tibetan tectonic evolution. *Earth and Planetary Science Letters* 205, 185–194.
- Lee, H.Y., Chung, S.L., Lo, C.H., Ji, J., Lee, T.Y., Qian, Q., Zhang, Q., 2009. Eocene Neotethyan slab breakoff in southern Tibet inferred from the Linzizong volcanic record. *Tectonophysics* 477, 20–35.
- Lee, H.Y., Chung, S.L., Ji, J., Qian, Q., Gallet, S., Lo, C.H., Lee, T.Y., Zhang, Q., 2012. Geochemical and Sr-Nd isotopic constraints on the genesis of the Cenozoic Linzizong volcanic successions, southern Tibet. *Journal of Asian Earth Sciences* 53, 96–114.
- Leech, M.L., Singh, S., Jain, A.K., Klemperer, S.L., Manickavasagam, R.M., 2005. The onset of India-Asia continental collision: early, steep subduction required by the timing of UHP metamorphism in the western Himalaya. *Earth and Planetary Science Letters* 234, 83–97.
- Li, Z.H., Zheng, L.L., Li, M.J., Xia, X.B., 2008. Petrological and Geochemical Characteristics of the Linzizong Volcanic Rocks in the Central Gangdese Area. *Bulletin of Mineralogy, Petrology and Geochemistry* 27, 20–27.
- Liang, X.R., Wei, G.J., Li, X.H., Liu, Y., 2003. Precise measurement of $^{143}\text{Nd}/^{144}\text{Nd}$ and Sm/Nd ratios using multiple-collectors inductively coupled plasma-mass spectrometer (MC-ICPMS). *Geochimica* 32, 91–96.
- Liang, Y.H., Chung, S.L., Liu, D., Xu, Y., Wu, F.Y., Yang, J.H., Wang, Y., Lo, C.H., 2008. Detrital zircon evidence from Burma for reorganization of the eastern Himalayan river system. *American Journal of Science* 308, 618–638.
- Liu, G., Einsele, G., 1994. Sedimentary history of the Tethyan basin in the Tibetan Himalayas. *Geologische Rundschau* 83, 32–61.
- Liu, S., Hu, R.Z., Gao, S., Feng, C.X., Huang, Z., Lai, S., Yuan, H., Liu, X., Coulson, I.M., Feng, G., 2009. U-Pb zircon, geochemical and Sr-Nd-Hf isotopic constraints on the age and origin of Early Palaeozoic I-type granite from the Tengchong-Baoshan Block, Western Yunnan Province, SW China. *Journal of Asian Earth Sciences* 36, 168–182.
- Ludwig, K., 2001. SQUID 1.12: A User's Manual. A Geochronological Toolkit for Microsoft Excel. Berkeley Geochronology Center Special Publication 1–22.
- Machado, N., Simonetti, A., 2001. U-Pb dating and Hf isotopic composition of zircon by laser-ablation-MC-ICP-MS. *Laser Ablation ICPMS in the Earth Sciences: Principles and Applications, Short Course, Mineralogical Association of Canada*, 29, pp. 121–146.
- Metcalfe, I., 1996a. Gondwanaland dispersion, Asian accretion and evolution of eastern Tethys*. *Australian Journal of Earth Sciences* 43, 605–623.
- Metcalfe, I., 1996b. Pre-Cretaceous evolution of SE Asian terranes. *Geological Society, London, Special Publications* 106, 97–122.
- Metcalfe, I., 1998. Palaeozoic and Mesozoic geological evolution of the SE Asian region: multidisciplinary constraints and implications for biogeography. *Biogeography and geological evolution of SE Asia*. 25–41.
- Middlemost, E.A.K., 1994. Naming materials in the magma/igneous rock system. *Earth-Science Reviews* 37, 215–224.
- Mitchell, A.H.G., 1981. Phanerozoic plate boundaries in mainland SE Asia, the Himalayas and Tibet. *Journal of the Geological Society* 138, 109–122.
- Mitchell, A.H.G., 1993. Cretaceous-Cenozoic tectonic events in the western Myanmar (Burma)-Assam region. *Journal of the Geological Society* 150, 1089–1102.
- Mo, X.X., Zhao, Z.D., Zhou, S., Dong, G.C., Guo, T., Wang, L., 2002. Evidence for timing of the initiation of India-Asia collision from igneous rocks in Tibet. *AGU Fall Meeting Abstracts*, p. 1201.
- Mo, X.X., Dong, G.C., Zhao, Z.D., Zhou, S., Wang, L.L., Qiu, R.Z., Zhang, F.Q., 2005. Spatial and temporal distribution and characteristics of granitoids in the Gangdese, Tibet and implication for crustal growth and evolution. *Geological Journal of China Universities* 11, 281–290.
- Mo, X.X., Hou, Z.Q., Niu, Y.L., Dong, G.C., Qu, X.M., Zhao, Z.D., Yang, Z.M., 2007. Mantle contributions to crustal thickening during continental collision: evidence from Cenozoic igneous rocks in southern Tibet. *Lithos* 96, 225–242.
- Mo, X.X., Niu, Y.L., Dong, G.C., Zhao, Z.D., Hou, Z.Q., Zhou, S., Ke, S., 2008. Contribution of syncollisional felsic magmatism to continental crust growth: a case study of the Paleogene Linzizong volcanic Succession in southern Tibet. *Chemical Geology* 250, 49–67.
- Mo, X.X., Dong, G.C., Zhao, Z.D., Zhu, D.C., Zhou, S., Niu, Y.L., 2009. Mantle input to the crust in southern Gangdese, Tibet, during the Cenozoic: zircon Hf isotopic evidence. *Journal of Earth Science* 20, 241–249.
- Molnar, P., Tapponnier, P., 1975. Cenozoic tectonics of Asia: effects of a continental collision. *Science* 189, 419–426.
- Morley, C., Woganan, N., Sankumarn, N., Hoon, T., Alief, A., Simmons, M., 2001. Late Oligocene–Recent stress evolution in rift basins of northern and central Thailand: implications for escape tectonics. *Tectonophysics* 334, 115–150.
- Najman, Y., Carter, A., Oliver, G., Garzanti, E., 2005. Provenance of Eocene foreland basin sediments, Nepal: constraints to the timing and diachroneity of early Himalayan orogenesis. *Geology* 33, 309–312.
- Najman, Y., Appel, E., Boudagher-Fadel, M., Bown, P., Carter, A., Garzanti, E., Godin, L., Han, J., Liebke, U., Oliver, G., 2010. Timing of India-Asia collision: geological, biostratigraphic, and palaeomagnetic constraints. *Journal of Geophysical Research* 115, B12416.
- Pan, G.T., Wang, L.Q., Li, R.S., Yuan, S.H., Ji, W.H., Yin, F.G., Zhang, W.P., Wang, B.D., 2012. Tectonic evolution of the Qinghai-Tibet Plateau. *Journal of Asian Earth Sciences*. <http://dx.doi.org/10.1016/j.jseas.2011.12.018>.
- Patriat, P., Achache, J., 1984. India-Eurasia collision chronology has implications for crustal shortening and driving mechanism of plates. *Nature* 311, 615–621.
- Pearce, J.A., Harris, N.B.W., Tindle, A.G., 1984. Trace element discrimination diagrams for the tectonic interpretation of granitic rocks. *Journal of Petrology* 25, 956–983.
- Peng, T.P., Wang, Y.J., Fan, W.M., Liu, D.Y., Shi, Y.R., Miao, L.C., 2006. SHRIMP zircon U-Pb geochronology of early Mesozoic felsic igneous rocks from the southern Lancangjiang and its tectonic implications. *Science in China Series D: Earth Sciences* 49, 1032–1042.
- Pitcher, W.S., 1982. Granite type and tectonic environment. In: Hsü, K.J. (Ed.), *Mountain Building Processes*. Academic Press, London, pp. 19–40.
- Rapp, R.P., Watson, E.B., 1995. Dehydration melting of metabasalt at 8–32 kbar: implications for continental growth and crust–mantle recycling. *Journal of Petrology* 36, 891–931.
- Replumaz, A., Tapponnier, P., 2003. Reconstruction of the deformed collision zone between India and Asia by backward motion of lithospheric blocks. *Journal of Geophysical Research* 108, 2285.
- Rickwood, P.C., 1989. Boundary lines within petrologic diagrams which use oxides of major and minor elements. *Lithos* 22, 247–263.
- Rowley, D.B., 1996. Age of initiation of collision between India and Asia: a review of stratigraphic data. *Earth and Planetary Science Letters* 145, 1–13.
- Rudnick, R., Gao, S., 2003. Composition of the continental crust. *Treatise on Geochemistry* 3, 1–64.
- Schärer, E., Munker, C., Mezger, K., 2001. Calibration of the lutetium–hafnium clock. *Science* 293, 683–687.
- Searle, M.P., 1996. Geological evidence against large-scale pre-Holocene offsets along the Karakoram fault: implications for the limited extrusion of the Tibetan Plateau. *Tectonics* 15, 171–186.
- Searle, M.P., 2006. Role of the Red River Shear zone, Yunnan and Vietnam, in the continental extrusion of SE Asia. *Journal of the Geological Society* 163, 1025–1036.
- Searle, M.P., Windley, B.F., Coward, M.P., Cooper, D.J.W., Rex, A.J., Rex, D.C., Tingdong, L., Xuchang, X., Jan, M.Q., Thakur, V.C., 1987. The closing of Tethys and the tectonics of the Himalaya. *Geological Society of America Bulletin* 98, 678–701.
- Searle, M.P., Noble, S., Cottle, J., Waters, D., Mitchell, A., Hlaing, T., Horstwood, M., 2007. Tectonic evolution of the Mogok metamorphic belt, Burma (Myanmar) constrained by U-Th-Pb dating of metamorphic and magmatic rocks. *Tectonics* 26, TC3014.
- Shi, G.R., Archbold, N.W., 1998. Permian marine biogeography of SE Asia. *Biogeography and Geological Evolution of SE Asia*. Backhuys, Leiden 57–72.
- Shi, G.R., Archbold, N.W., Zhan, L.P., 1995. Distribution and characteristics of mixed (transitional) mid-Permian (Late Artinskian–Ufimian) marine faunas in Asia and their palaeogeographical implications. *Palaeogeography, Palaeoclimatology, Palaeoecology* 114, 241–271.
- Singer, B.S., Myers, J.D., Frost, C.D., 1992. Mid-Pleistocene lavas from the Seguan volcanic center, central Aleutian arc: closed-system fractional crystallization of a basalt to rhyodacite eruptive suite. *Contributions to Mineralogy and Petrology* 110, 87–112.
- Socquet, A., Pubellier, M., 2005. Cenozoic deformation in western Yunnan (China–Myanmar border). *Journal of Asian Earth Sciences* 24, 495–515.
- Song, S., Niu, Y., Wei, C., Ji, J., Su, L., 2010. Metamorphism, anatexis, zircon ages and tectonic evolution of the Gongshan block in the northern Indochina continent—An eastern extension of the Lhasa Block. *Lithos* 120, 327–346.
- Streckeisen, A., 1976. To each plutonic rock its proper name. *Earth-Science Reviews* 12, 1–33.
- Sun, S.S., McDonough, W.F., 1989. Chemical and isotopic systematics of oceanic basalts: implication for mantle composition and process. *Geological Society, London, Special Publications* 42, 313–345.
- Sun, Z.M., Pei, J.L., Li, H.B., Xu, W., Jiang, W., Zhu, Z.M., Wang, X.S., Yang, Z.Y., 2012. Palaeomagnetism of late Cretaceous sediments from southern Tibet: evidence for the consistent palaeolatitudes of the southern margin of Eurasia prior to the collision with India. *Gondwana Research* 21, 53–63.
- Sylvester, P.J., 1998. Post-collisional strongly peraluminous granites. *Lithos* 45, 29–44.
- Tan, X., Gilder, S., Kodama, K.P., Jiang, W., Han, Y., Zhang, H., Xu, H., Zhou, D., 2010. New paleomagnetic results from the Lhasa block: revised estimation of latitudinal shortening across Tibet and implications for dating the India-Asia collision. *Earth and Planetary Science Letters* 293, 396–404.
- Tapponnier, P., Lacassin, R., Leloup, H., Schärer, U., Zhong, D., Liu, X., Ji, S., Zhang, L., Zhong, J., 1990. The Ailao Shan–Red River metamorphic belt: tertiary left-lateral shear between Indochina and South China. *Nature* 343, 431–437.
- Taylor, S.R., McLennan, S.M., 1985. *The Continental Crust: Its Composition and Evolution*. Blackwell Scientific Publications, Palo Alto, CA 1–328.
- Ueno, K., 2000. Permian fusulinacean faunas of the Sibumasu and Baoshan Blocks: implications for the paleogeographic reconstruction of the Cimmerian continent. *Geosciences Journal* 4, 160–163.

- Ueno, K., 2003. The Permian fusulinoidean faunas of the Sibumasu and Baoshan blocks: their implications for the paleogeographic and paleoclimatologic reconstruction of the Cimmerian Continent. *Palaeogeography, Palaeoclimatology, Palaeoecology* 193, 1–24.
- Wang, Y., 1983. The characteristics and significance of Carboniferous gravel beds in the Tengchong and Baoshan area, western Yunnan. In: Zhou, Z., Xu, X., Zhou, W. (Eds.), *Geology of Qinghai–Xizang (Tibet) Plateau*: Beijing, 11, pp. 71–77 (in Chinese with English abstract).
- Wang, E., Burchfiel, B., 1997. Interpretation of Cenozoic tectonics in the right-lateral accommodation zone between the Ailao Shan shear zone and the eastern Himalayan syntaxis. *International Geology Review* 39, 191–219.
- Wang, Y.J., Fan, W.M., Zhang, Y.H., Peng, T., Chen, X.Y., Xu, Y.G., 2006. Kinematics and $^{40}\text{Ar}/^{39}\text{Ar}$ geochronology of the Gaoligong and Chongshan shear systems, western Yunnan, China: implications for early Oligocene tectonic extrusion of SE Asia. *Tectonophysics* 418, 235–254.
- Wang, Y.J., Fan, W.M., Sun, M., Liang, X., Zhang, Y.H., Peng, T.P., 2007. Geochronological, geochemical and geothermal constraints on petrogenesis of the Indosinian peraluminous granites in the South China Block: a case study in the Hunan Province. *Lithos* 96, 475–502.
- Wang, J.G., Hu, X.M., Jansa, L., Huang, Z.C., 2011. Provenance of the Upper Cretaceous–Eocene deep-water sandstones in Sangdanlin, southern Tibet: constraints on the timing of initial India–Asia collision. *Journal of Geology* 119, 293–309.
- Wei, G.J., Liang, X.R., Li, X.H., Liu, Y., 2002. Precise measurement of Sr isotopic composition of liquid and solid base using (LP) MC-ICPMS. *Geochimica* 31, 295–299.
- Wen, D.R., Chung, S.L., Song, B., Iizuka, Y., Yang, H.J., Ji, J., Liu, D., Gallet, S., 2008a. Late Cretaceous Gangdese intrusions of adakitic geochemical characteristics, SE Tibet: petrogenesis and tectonic implications. *Lithos* 105, 1–11.
- Wen, D.R., Liu, D., Chung, S.L., Chu, M.F., Ji, J., Zhang, Q., Song, B., Lee, T.Y., Yeh, M.W., Lo, C.H., 2008b. Zircon SHRIMP U–Pb ages of the Gangdese Batholith and implications for Neotethyan subduction in southern Tibet. *Chemical Geology* 252, 191–201.
- Wilson, M., 1989. Igneous Petrogenesis. Chapman & Hall, London, UK 1–466.
- Wu, H., Boulter, C., Ke, B., Stow, D., Wang, Z., 1995. The Changning–Menglian suture zone: a segment of the major Cathaysian–Gondwana divide in Southeast Asia. *Tectonophysics* 242, 267–280.
- Xia, B., Lin, Q.C., Zhang, Y.Q., Liang, H., Xu, L., 2009. SHRIMP U–Pb dating of zircon from gneiss in the Tongmai region: evidence for the India Eurasia collision time. *Acta Geologica Sinica* 83, 347–352.
- Xia, L.Q., Li, X.M., Ma, Z.P., Xu, X.Y., Xia, Z.C., 2011a. Cenozoic volcanism and tectonic evolution of the Tibetan plateau. *Gondwana Research* 19, 850–866.
- Xia, X., Sun, M., Geng, H.Y., Sun, Y., Wang, Y., Zhao, G., 2011b. Quasi-simultaneous determination of U–Pb and Hf isotope compositions of zircon by excimer laser-ablation multiple-collector ICPMS. *Journal of Analytical Atomic Spectrometry* 26, 1868–1871.
- Xie, K.J., Zeng, L.S., Liu, J., Gao, L.E., HU, G.Y., 2011. Timing and geochemistry of the Linzizong Group volcanic rocks in Sangsang area, Ngamring County, southern Tibet. *Geological Bulletin of China* 30, 1139–1152 (in Chinese with English abstract).
- Xu, R.H., Schärer, U., Allègre, C.J., 1985. Magmatism and metamorphism in the Lhasa block (Tibet): a geochronological study. *Journal of Geology* 41–57.
- Xu, Y.G., Lan, J.B., Yang, Q.J., Huang, X.L., Qiu, H.N., 2008. Eocene break-off of the Neo-Tethyan slab as inferred from intraplate-type mafic dykes in the Gaoligong orogenic belt, eastern Tibet. *Chemical Geology* 255, 439–453.
- Xu, Y.G., Yang, Q.J., Lan, J.B., Luo, Z.Y., Huang, X.L., Shi, Y.R., Xie, L.W., 2012. Temporal-spatial distribution and tectonic implications of the batholiths in the Gaoligong–Tengliang–Yingjiang area, western Yunnan: constraints from zircon U–Pb ages and Hf isotopes. *Journal of Asian Earth Sciences* 53, 151–175.
- Yang, Q.J., Xu, Y.G., Huang, X.L., Luo, Z.Q., Shi, Y.R., 2009. Geochronology and geochemistry of granites in the Tengliang area, western Yunnan: tectonic implication. *Acta Petrologica Sinica* 25, 1092–1104.
- Ye, M.F., Li, X.H., Li, W.X., Liu, Y., Li, Z.X., 2007. SHRIMP zircon U–Pb geochronological and whole-rock geochemical evidence for an early Neoproterozoic Sibaao magmatic arc along the southeastern margin of the Yangtze Block. *Gondwana Research* 12, 144–156.
- Yi, Z., Huang, B., Chen, J., Chen, L., Wang, H., 2011. Paleomagnetism of early Paleogene marine sediments in southern Tibet, China: implications to onset of the India–Asia collision and size of Greater India. *Earth and Planetary Science Letters* 309, 153–165.
- Yin, A., 2006. Cenozoic tectonic evolution of the Himalayan orogen as constrained by along-strike variation of structural geometry, exhumation history, and foreland sedimentation. *Earth-Science Reviews* 76, 1–131.
- Yin, A., Harrison, T.M., 2000. Geologic evolution of the Himalayan–Tibetan orogen. *Annual Review of Earth and Planetary Sciences* 28, 211–280.
- Yuan, H.L., Gao, S., Liu, X.M., Li, H.M., Gunther, D., Wu, F.Y., 2004. Accurate U–Pb age and trace element determinations of zircon by laser ablation inductively coupled plasma mass spectrometry. *Geostandards and Geoanalytical Research* 28, 353–370.
- Yunnan BGMR (Yunnan Bureau of Geology and Mineral Resources, 1990. *Regional Geology of the Yunnan Province*. Geological Publishing House, Beijing 592 (in Chinese with English abstract).
- Zaw, K., 1990. Geological, petrological and geochemical characteristics of granitoid rocks in Burma: with special reference to the associated W–Sn mineralization and their tectonic setting. *Journal of Southeast Asian Earth Sciences* 4, 293–335.
- Zen, E., 1986. Aluminum enrichment in silicate melts by fractional crystallization: some mineralogic and petrographic constraints. *Journal of Petrology* 27, 1095–1117.
- Zhang, B., Zhang, J., Zhong, D., 2010a. Structure, kinematics and ages of transpression during strain-partitioning in the Chongshan shear zone, western Yunnan, China. *Journal of Structural Geology* 32, 445–463.
- Zhang, L.L., Zhu, D.C., Zhao, Z.D., Dong, G.C., Mo, X.X., Guan, Q., Liu, M., Liu, M.H., 2010b. Petrogenesis of magmatism in the Baerda region of Northern Gangdese, Tibet: constraints from geochemistry, geochronology and Sr–Nd–Hf isotopes. *Acta Petrologica Sinica* 26, 1871–1888 (in Chinese with English abstract).
- Zhang, Z.M., Zhao, G.C., Santosh, M., Wang, J.L., Dong, X., Shen, K., 2010c. Late Cretaceous charnockite with adakitic affinities from the Gangdese batholith, southeastern Tibet: evidence for Neo-Tethyan mid-ocean ridge subduction? *Gondwana Research* 17, 615–631.
- Zhang, Z.M., Zhao, G.C., Santosh, M., Wang, J.L., Dong, X., Liou, J.G., 2010d. Two-stages of granulite-facies metamorphism in the eastern Himalayan syntaxis, south Tibet: petrology, zircon geochronology and implications for the subduction of Neo-Tethys and the Indian continent beneath Asia. *Journal of Metamorphic Geology* 28, 719–733.
- Zhang, B., Zhang, J.J., Zhong, D.L., Wang, X.X., Qu, J.F., Guo, L., 2011. Structural feature and its significance of the northernmost segment of the Tertiary Biluoqueshan–Chongshan shear zone, east of the Eastern Himalayan Syntaxis. *Science China Earth Sciences* 54, 959–974 (in Chinese with English abstract).
- Zhang, B., Zhang, J., Zhong, D., Yang, L., Yue, Y., Yan, S., 2012. Polystage deformation of the Gaoligong metamorphic zone: structures, $^{40}\text{Ar}/^{39}\text{Ar}$ mica ages, and tectonic implications. *Journal of Structural Geology* 37, 1–18.
- Zhong, D., 1998. Paleo-Tethyan orogenic belt in the western parts of the Sichuan and Yunnan Provinces. Science Press, Beijing 1–231 (in Chinese with English abstract).
- Zhu, D.C., Pan, G.T., Mo, X.X., Duan, L., Liao, Z.L., 2004. The age of collision between India and Eurasia. *Advances in Earth Science* 19, 564–571 (in Chinese with English abstract).
- Zhu, D.C., Mo, X.X., Niu, Y., Zhao, Z.D., Wang, L.Q., Pan, G.T., Wu, F.Y., 2009a. Zircon U–Pb dating and in-situ Hf isotopic analysis of Permian peraluminous granite in the Lhasa terrane, southern Tibet: implications for Permian collisional orogeny and paleogeography. *Tectonophysics* 469, 48–60.
- Zhu, D.C., Mo, X.X., Wang, L.Q., Zhao, Z.D., Niu, Y.L., Zhou, C.Y., Yang, Y.H., 2009b. Petrogenesis of highly fractionated I-type granites in the Chayu area of eastern Gangdese, Tibet: constraints from zircon U–Pb geochronology, geochemistry and Sr–Nd–Hf isotopes. *Science in China Series D: Earth Sciences* 39, 833–848 (in Chinese with English abstract).
- Zhu, D.C., Zhao, Z.D., Niu, Y., Mo, X.X., Chung, S.L., Hou, Z.Q., Wang, L.Q., Wu, F.Y., 2011. The Lhasa Terrane: record of a microcontinent and its histories of drift and growth. *Earth and Planetary Science Letters* 301, 241–255.
- Zhu, D.C., Zhao, Z.D., Niu, Y.L., Dilek, Y., Hou, Z.Q., Mo, X.X., 2013. The origin and pre-Cenozoic evolution of the Tibetan Plateau. *Gondwana Research* 23, 1429–1454.